AD_____

Award Number: W81XWH-14-1-0295

TITLE: Microenvironments and Signaling Pathways Regulating Early Dissemination, Dormancy, and Metastasis

PRINCIPAL INVESTIGATOR: Julio A. Aguirre-Ghiso

CONTRACTING ORGANIZATION: Mount Sinai School of Medicine
New York, NY 10029

REPORT DATE: September 2015

TYPE OF REPORT: Annual

PREPARED FOR: U.S. Army Medical Research and Materiel Command
Fort Detrick, Maryland 21702-5012

REPORT DOCUMENTATION PAGE

Form Approved
OMB No. 0704-0188

1. REPORT DATE	**2. REPORT TYPE**	**3. DATES COVERED**
September 2015	Annual	1 Sep 2014 - 31 Aug 2015

4. TITLE AND SUBTITLE
Microenvironments and Signaling Pathways Regulating Early Dissemination, Dormancy, and Metastasis.

5a. CONTRACT NUMBER

5b. GRANT NUMBER
W81XWH-14-1-0295

5c. PROGRAM ELEMENT NUMBER

6. AUTHOR(S)
Julio Aguirre-Ghiso, John Condeelis

E-Mail: Julio.aguirre-ghiso@mssm.edu

5d. PROJECT NUMBER

5e. TASK NUMBER

5f. WORK UNIT NUMBER

7. PERFORMING ORGANIZATION NAME(S) AND ADDRESS(ES)

Mount Sinai, School of Medicine,
New York, NY, 10029

8. PERFORMING ORGANIZATION REPORT NUMBER

9. SPONSORING / MONITORING AGENCY NAME(S) AND ADDRESS(ES)
U.S. Army Medical Research and Materiel Command
Fort Detrick, Maryland 21702-5012

10. SPONSOR/MONITOR'S ACRONYM(S)

11. SPONSOR/MONITOR'S REPORT NUMBER(S)

12. DISTRIBUTION / AVAILABILITY STATEMENT
Approved for Public Release; Distribution Unlimited

13. SUPPLEMENTARY NOTES
NA

14. ABSTRACT

We devoted majority of the effort to SA1 and optimizing methods that impact both aims. SA1 is to understand the intrinsic mechanisms of dissemination by early-progressed cancer cells and how the microenvironment in these primary sites named P-TMEM (**P**rimary **T**umor **M**icro**e**nvironment of **M**etastases) contribute to early dissemination. We now have new data suggesting that a signature of early dissemination markers consisting on $HER2^{HI}$/p-$ATF2^{LO}$/E-$cadh^{LO}$ could identify motile early-progressed tumor cells and predict for dissemination. We further show that mammary tissue macrophages and $HER2^{HI}$/p-$ATF2^{LO}$/E-$cadh^{LO}$ tumor cells cooperate to disseminate early. This further supports our hypothesis that even in early cancer lesions macrophages and tumor cells assemble with endothelial cells a TMEM structure. We have also made progress in generating a standardized triple staining that captures all these cell types in all tissues and we have been able to document using intravital imaging the process of intravasation in early cancer lesions. Our work revealed that the presence of intraepithelial macrophages in DCIS samples could accurately predict dissemination in 70% of the cases of patients with bone marrow DTCs (**D**isseminated **T**umor **C**ells). SA2 focuses on elucidate how S-TMEM (**S**econdary **T**umor **M**icro**e**nvironment of **M**etastases) contributes to the dormancy phase of early DTCs. Our new data show that depletion of macrophages during early dissemination steps significantly reduces metastasis that develop into the late stages of progression, providing functional support for macrophages in P- and S-TMEM structures in metastasis development. We also found that early DTCs appear to undergo a p38 independent dormancy and remain mesenchymal in secondary organs. In contrast, in animals with overt tumors p38 inhibition resulted in an awakening of dormant DTCs in lungs, that now have a mixture of early and late disseminated tumor cells. Progress has also been made in devising a sorting protocol to isolate CFP+/HER2+ DTCs from lungs and CTCs in the MMTV-Neu-CFP model and we have also devised new strategies to identify the early and late gene signatures in DTCs proposed in our grant. Overall we have made significant progress and we do not foresee having to alter our specific aims in any way.

15. SUBJECT TERMS

dormancy, early dissemination, EMT, macrophages, TMEM

16. SECURITY CLASSIFICATION OF:			**17. LIMITATION OF ABSTRACT**	**18. NUMBER OF PAGES**	**19a. NAME OF RESPONSIBLE PERSON**
a. REPORT	**b. ABSTRACT**	**c. THIS PAGE**			USAMRMC
U	U	U	UU		**19b. TELEPHONE NUMBER** *(include area code)*

Table of Contents

INTRODUCTION

Understanding early dissemination and early DTC behavior is important because we found that DCIS lesions produce large amounts of early DTCs that are dormant. This could contribute silently to therapy resistance and late metastatic relapse. Unfortunately, these events have remained understudied because of lack of tools. Our collaboration, which brings new tools, has allowed us to explore these mechanisms to gather this highly significant and transformative knowledge. We believe that our proposal will provide answers to the **overarching challenge** to *"Determine why/how breast cancer cells lay dormant for years and then re-emerge (recurrence); determine how to eliminate dormant cells early".*

We proposes the existence of a structure called tumor microenvironment of metastasis or TMEM, which is composed by a specialized macrophage a tumor cell also specialized and the endotghelium[1]. We detected primary tumor or **P-TMEM** (previously only detected in invasive cancers) in pre-malignant lesions[1]. The P-TMEM is required to induce an EMT and early dissemination of pre-malignant MECs. We further hypothesize that after extravasation at S-TMEM, in order to exit dormancy a stable **S-TMEM** structure needs to be maintained and that early DTCs cannot sustain its assembly possibly because they lack a persistent MΦ recruiting program. Our *rationale* is that by understanding early dissemination and dormancy of DTCs we will find ways to eradicate dormant DTCs and prevent metastasis.

Our original specific aims are 1. Test how ErbB2^{high}/P-p38^{low} MECs assemble P-TMEM during early dissemination. 2. Test the role of S-TMEM in regulating early DTC dormancy.

In this progress report we provide novel evidence supporting our aims and hypothesis.

PROGRESS REPORT- DoD grant Number: W81XWH-14-1-0295

Title: Microenvironments and Signaling Pathways Regulating Early Dissemination, Dormancy, and Metastasis.

Introduction: We provide a summary of the original aims, their rationale and specific progress (see Results section) focused on the tasks set for this proposal. At the end of the Results we list the additional tasks that will be expanded for the next year.

Original Specific Aim 1- To test how ErbB2high/P-p38low MECs assemble P-TMEM during early dissemination.

SA1.1. Objective: use intravital imaging and MMTV-ErbB2-CFP, MMTV-PyMT-EGFP-c-fms-CFP transgenic mice and modulation of ErbB2 and p38 signaling to detect P-TMEM function during intravasation of "early" and "late" ErbB2+ MECs.

Results: We had proposed to image live the process of intravasation using MMTV-Neu-**CFP** (**c**yan **f**luorescent **p**rotein) mice, which would further confirm the CTC and DTC results in situ. We initiated the intravital imaging of mammary glands of MMTV-Neu-CFP females at early stages to detect the motility of these early cancer cells. This was done by collecting movies from DMSO-treated mice and mice treated with i.p. with a p38 inhibitor SB203580 (10 mg/kg, every 48 hrs., at 2 and 4 weeks of treatment[2]).

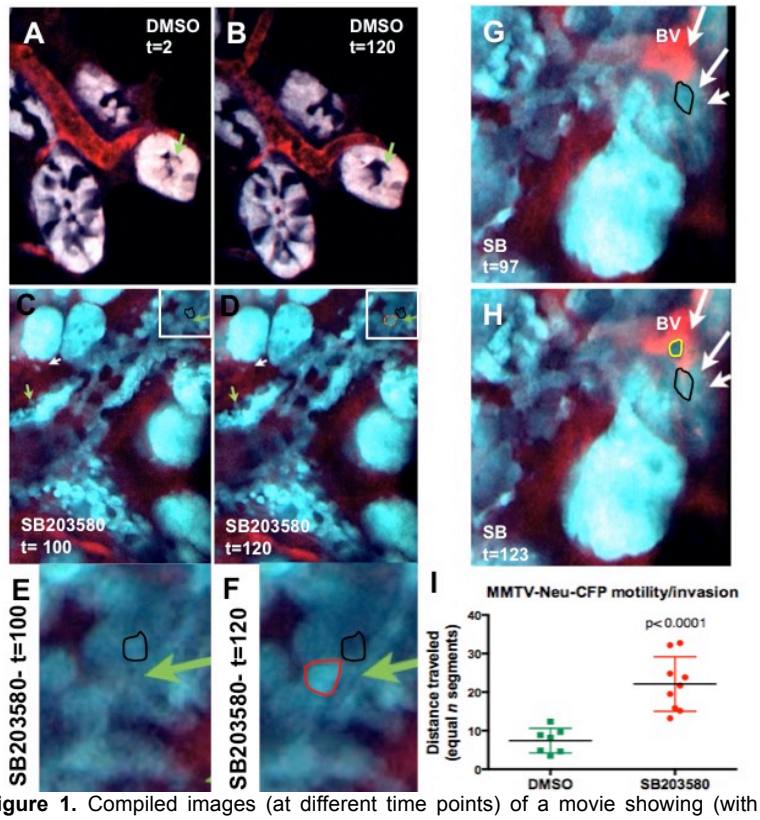

Figure 1. Compiled images (at different time points) of a movie showing (with green arrow) the movement of a single CFP+ cell inside a duct in DMSO-treated mouse (**A** and **B**) and 3 different CFP+ cells (green and white arrows) in SB-treated mouse (**C, D, E, F, G** and **H**). **E** and **F** are zoomed in regions marked in a white square in **C** and **D**, respectively. Note the disorganized structures in SB-treated mouse. G and H. Images show the translocation of a CFP+ cells over time into a blood vessel (BV) in a SB-treated MMTV-Neu-CFP mouse. **I**. Measurements of distance traveled for each single MMTV-Neu-CFP MECs upon treatment. Distance are measured in a time lapse of 2 hours. t=in minutes

Strategy followed to obtain steady movies of early dissemination in real time:
We performed a minimal surgery to expose the lower mammary glands directly over the microscope objective. This approach had several limitations including the continuum stretching and movement of the fat pad tissue that ultimately led to unstable images. To overcome the previous pitfall we decided to use the same devices already used in Dr. Condeelis's lab to image mammary glands[3]. In this case the thickness of the device avoided the direct contact of the fat pad with the glass leading to low-resolution images. Finally, we designed a new device, named flat mammary gland (MG) window, which consisted in a Teflon ring of an external diameter of 0.55 inches and a rounded glass sealed to the inner ring**.** Then, we glued it to the skin around the exposed mammary gland to finally mount it over the objective. Using this new flat MG window we were able to image pre-malignant

lesions for 2 hours and to obtain high quality steady movies of the mammary glands with single cell resolution (**Fig1**). These movies are now part of a submitted manuscript under review in Cancer Cell and reported in the Reportable Outcomes section (See appendix).

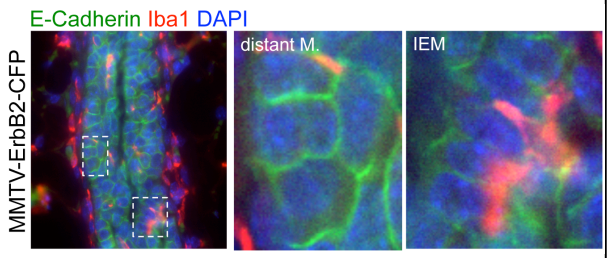

Figure 2. Paraffin embedded sections of 7 week old MMTV-ErbB2-CFP mammary glands were stained for E-Cadherin and the macrophage marker Iba1. Detail on the right shows that E-Cadherin is disrupted and reduced in early cancer cells adjacent to intra-epithelial macrophages.

Once the pre-malignant lesion was identified in the CFP+ mammary gland we i.v. injected (tail vein) a dextran-TRITC solution for the visualization of blood vessels. Then, we proceeded to analyze 3 different regions and collect images for each one at interval of 2 minutes. For each region we did z-stack of 5 um with a total of 9 different sections per region. After we reached approximately 2 hours average for each region we imaged another 3 different regions. At the end of the experiment we processed these images using the Image J software to generate movies. Careful analysis of the movies revealed that while in DMSO-treated mouse pre-malignant cancer cells did not present micro-invasive behavior into the stroma at early stages (10 weeks) later time points revealed spontaneous early dissemination (**Fig1**). Importantly, SB203580-treated mice showed a significant increase in ductal cell motility. This was observed as intra-ductal movement within the disorganized ducts (**See appendix**). We quantified the distance travelled by each cell in DMSO or SB-treated mice (**See appendix**) and concluded that SB-treated cancer cells displayed enhanced motility. We were able to detect translocation and local movement of single cells within the ducts (**Fig1**).

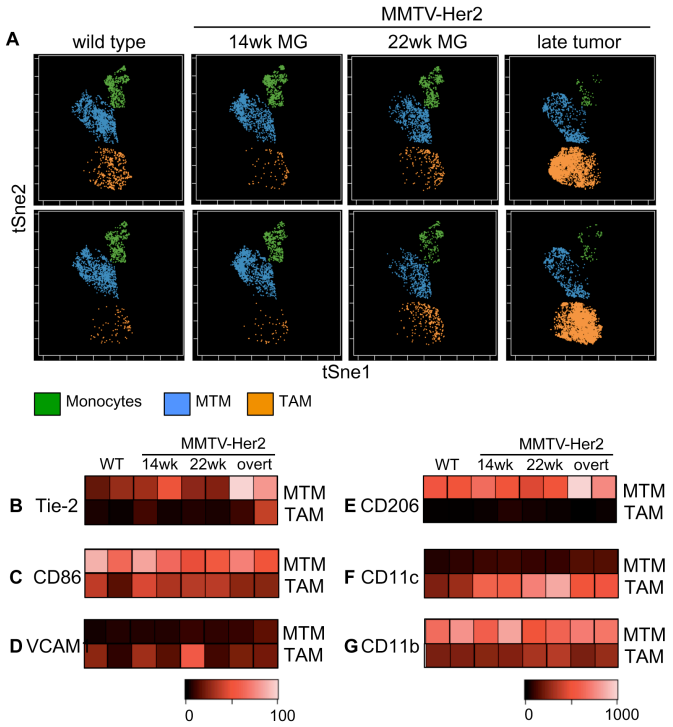

Figure 3. Phenotypic profiling of macrophages in early mammary cancer lesions. Whole mammary glands from FVB wild type mice or 14 and 20 week old pre-malignant MMTV-ErbB2 mice and invasive tumors from MMTV-ErbB2 mice were analyzed by mass cytometry against 36 markers. To analyze macrophages and monocytes, we gated out doublets, dead cells, non-hematopoietic cells (CD45), non T- and B-Cells (CD4, CD19) and non-neutrophils (Gr1) and then analyzed CD64+ CD1b+ cells. A: Visne plots of Ly6C+ monocytes, CD206+ mammary tissue macrophages (MTMs) and VCAM+ tumor associated macrophages (TAMs). Two individual animals per group were analyzed (top and bottom row). B-G: Heat plot analysis for different markers in the identified subpopulations are shown.

More importantly we were able to detect events where single CFP+ cells entered blood vessels neighboring the lesions and were carried away by the blood stream (**Fig. 1 G** and **H**). These events were not seen in the DMSO-treated animals analyzed. This confirms the enhanced intravasating capacity of Neu+/p38^{lo} cells when p38 inhibitor is present as deduced from the CTC and DTC analysis (**See appendix**). Of interest, we noticed less tight assembly of ductal and acinar structures when p38 was inhibited. This may be indicative of an EMT that was detected in these cells and anoikis resistance. It may also be the consequence of macrophages assembling P-TMEM and further enhancing the EMT (**See below**). In addition, the vasculature in SB-treated mice appeared less patent since dextran-TRITC was observed leaked out and taken by macrophages.

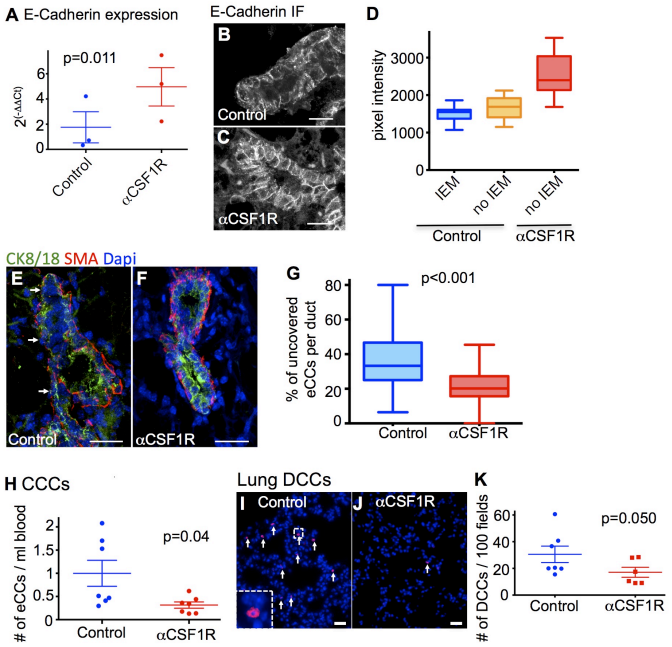

Figure 4. Macrophage depletion during pre-malignant stages prevents early cancer cell dissemination. 20 week old pre-malignant MMTV-ErbB2 mice were treated with the anti CSF-1Ra ASF98 antibody and animals were harvested after two weeks with no signs of invasive carcinoma. E-Cadherin expression in whole mammary glands was determined by immunofluoresence staining against E-Cadherin of mammary gland sections (A) and RealTime PCR of whole mammary gland lysates (B). E-Cadherin signal intensity was measured in regions of cell junctions, dependent on the presence of intra-epithelial macrophages (IEM) (D). Pre-malignant mammary glands were stained against (E,F) and the percentage of early cancer cells not covered by myoepithelium was quantified (G). Circulating early cancer cells were quantified by harvesting peripheral blood and determining the amount of ErbB2 and CK8/18 positive eCCs per mL blood (H). Disseminated early cancer cells were quantified by staining lung sections against ErbB2 (I,K) and quantifying the average of ErbB2+ cells per 100 fields (K). CCCs, circulating cancer cells. DCCs disseminated cancer cells

We had also proposed to quantify TMEM in sections from pre-malignant MTV-Neu-CFP mice by looking at tumor cells, endothelial cells and macrophages to see whether TMEM structure already occur early during tumor progression. In preparation for these in vivo analyses, we stained macrophages in sections in MMTV-ErbB2-CFP mice and could reproduce our finding that macrophages enter pre-malignant mammary ducts (**Fig.2**). We also found that early cancer cells neighboring intra-epithelial macrophages show low levels of E-Cadherin (**Fig.2**), indicating that intra-epithelial macrophages might induce an EMT in pre-malignant MECs. We then analyzed the phenotype of macrophages in FVB wild type or pre-malignant MMTV-ErbB2 mammary glands as well as in MMTV-ErbB2 invasive tumors by mass flow cytometry (CyTOF – **Fig3**) and found that wild type and pre-malignant mice predominantly contained mammary tissue but not tumor-associated macrophages and that these mammary tissue macrophages matched the Tie2^{high}, CD11c^{low}, CD206^{+} signature of TMEM macrophages recently described for invasive tumors[4] (**Fig.3**) indicating that a P-TMEM which drives early dissemination might be functional in pre-malignant stages as well.

We next tested whether macrophages functionally contribute to early dissemination by depleting macrophages from pre-malignant MMTV-ErbB2 mice using an antibody against CSF1Rα for two weeks and sacrificed animals before these developed signs of invasive tumors. We found that macrophage depletion during pre-malignant stages restored overall E-Cadherin expression and E-Cadherin signal intensity (**Fig.4A-D**) and normalized the myoepithelium covering pre-malignant ducts **Fig.4E-G**). Importantly, the number of circulating MECs and disseminated MECs in the lung was significantly reduced when macrophages had been depleted (**Fig.4H-K**).

Conclusions: First we confirmed that inhibition of p38α/β signaling by treatment of the new MMTV-Neu-CFP mice with SB203580 recapitulated the previously effect shown in the MMTV-Neu mice (no tag). These results also revealed in real time and live imaging the dissemination process as never before documented. These data support the hypothesis that p38 inhibition favors a motile phenotype that propels early dissemination. These findings are part of 2 manuscripts now in the process of review (Appendix I and II). The additional evidence showed that intraepithelial macrophages also occur in the MMTV-Neu-CFP mice and we characterize these macrophages as mammary tissue macroiphages[5] and showed that these are vital for disrupting the ductal epithelial structures, favoring an EMT and favoring early dissemination.

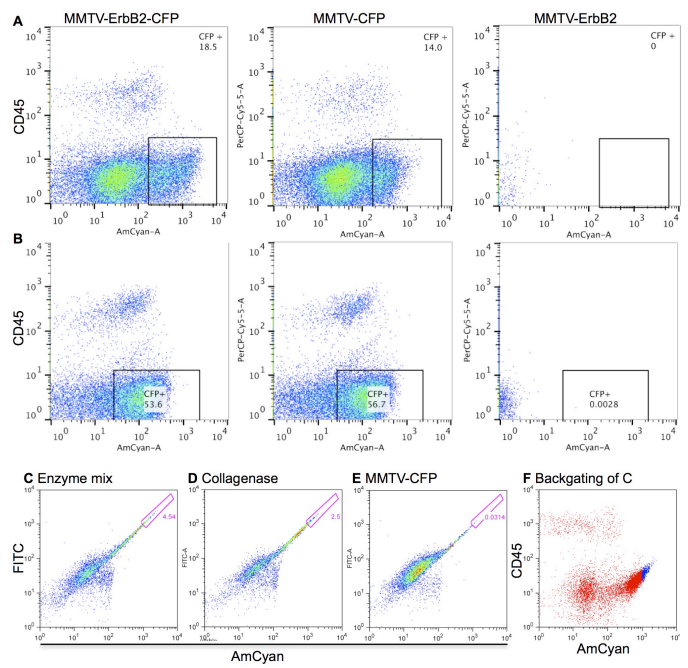

Figure 5. Detection of CFP+ tumor cells by flow cytometry. Mammary glands (A) and lungs (B) of MMTV-ErbB2-CFP mice were digested with collagenase and stained against CD45. After gating out doublets and dead cells, CFP signals were detected in the AmCyan channel and plotted against CD45 (PerCP-Cy5.5). To improve flow cytometry analysis, MMTV-ErbB2-CFP mammary glands were digested with the fatty tissue enzyme kit from Miltenyi (C,E) or with collagenase (D) and then all hematopoietic cells were depleted using the cell lineage depletion kit by Miltenyi. F: AmCyan+/FITC+ cells were backgated against CD45-PerCP-Cy5.5 signals to show that detected positive population is indeed of epithelial origin.

Plans for the coming year: We will quantify the number of events that show intravasation dynamics of pre-malignant MECs into blood vessels in DMSO- and SB-treated animals. Specifically, we will quantify speed, frequency and mode (single cells vs. cohorts and/or streaming) of local invasion and intravasation. So far our analysis has been performed with a resolution that enables us to detect single cells by doing z-stack of 5 um. We will increase the number of images taken per region to detect 1 um of thickness. With this type of resolution we will perform 3D reconstructions to detect with high quality the body and protrusions of any given cell. This undoubtedly will help us to identify the whole cell along its trajectory. Once we have established the optimal settings for visualization in vivo we will proceed by using the MMTV-PyMT-EGFP-c-fms-CFP mouse model. The latter, will allow us to detect the interactions of macrophages (CFP) with tumor cells (GFP). We are also optimizing the triple staining detect TMEM structures by IHC and this will allow unifying our methods wit h the Condeelis lab that we can then use as standardized measure of P-TMEM and S-TMEM quantification as reported.[1]

<u>SA1.2. Goal:</u> obtain expression profiles from early and late CTCs to identify genes involved in MΦ recruitment and dormancy onset.

Results: In order to isolate CTCs (also termed circulating cancer cells, CCCs) by FACS, we initiated the optimization of flow cytometric detection of tumor cells in the MMTV-ErbB2-CFP model. A population of CFP+ cells could be detected in mammary glands of MMTV-ErbB2-CFP cells which was absent in MMTV-ErbB2 mice (**Fig.5A**). These CFP+ cells could also be detected in lungs of MMTV-ErbB2-CFP mice as well as MMTV-CFP mice but no in MMTV-ErbB2 mice (**Fig.5B**) which led us to the conclusion that the MMTV promoter must be also active in cells other than mammary epithelial cells since no CFP+ MECs should reach the lung in the absence of the ErbB2 oncogene. We are currently optimizing the flow cytometry conditions. So far we found that magnetic bead based cell depletion of hemtopoietic cells prior to flow analysis increases purity (**Fig. 5C**). Additionally, we are testing commercially available enzyme mixes instead of collagenase and found that the use of an enzyme mix leads to higher detection rates of CFP^{high} cells (**Fig.5C,D**) which are CD45- (**Fig.5F**) and which cannot be detected in MMTV-CFP mice. We are currently additionally testing HER2 antibodies in order to then isolate a pure population of MMTV-ErbB2-CFP+ MECs from the primary site as well as CTCs and DTCs in different target organs (SA2.3). Finally we are optimizing the detection of HER2 in single tumor cells using the C1 Fluidigm system to have as a backup in case the FACS method results problematic. This will allow isolating CFP+ cells by FACS profiling individual cells for HER2 status and then using the RNA from these cells for RNAseq. **<u>Conclusion</u>**: we conclude that the main components to isolate DTCs (see below) and CTCs to obtain the first early dissemination signature are in place and we are optimizing methods that will allow achieving this aim.

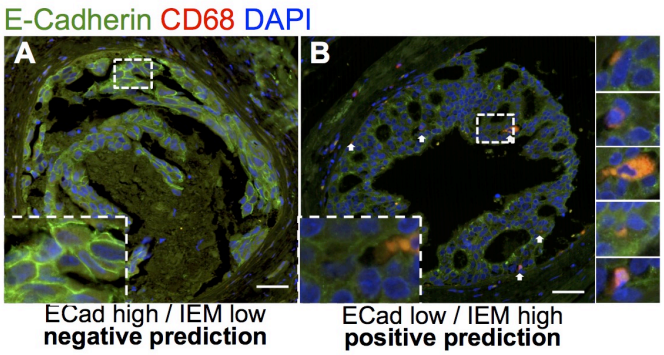

C

ECad	IEM	# of cases	prediction	positive for DCCs
high	low	10	positive	7
low	high	10	negative	5
Positive predictive value: 7/10 = 70%				

Figure 6. E-Cadherin and macrophage staining are indicative of early dissemination in DCIS patients. Sections from DCIS patients were bone marrow aspirates had been analyzed for the presence of DCCs were analyzed blindly. E-Cadherin and macrophages (CD68) were stained and patients were assessed as low risk when they had high E-Cadherin signals and low numbers of intra-epithelial macrophages (IEM) (A) or high risk when E-Cadherin signals were low and IEM numbers were high (B). From 20 analyzed cases, 10 were predicted to contain DTCs and 10 as being DTC negative. Unblinding revealed that for 7 out of 10 cases the presence of DTCs was predicted correctly, resulting in a positive predictive value of 70%.

Plans for the coming year: We will complete optimization of tumor cell detection (CTCs and DTCs) in these models and continue with the initial plan. The optimized antibody for tumor cell detection will be used in **SA2.2** (isolate early and late DTCs to determine their dormancy profiles and the mechanisms that distinguish their S-TMEM assembling potential).

SA1.3. Objective: To correlate early dissemination markers in primary breast tumors (DCIS and invasive lesions) with DTC presence in BM

Results*:* We first correlated the expression of ErbB2, E-cadherin and p-ATF2 in early lesions in MMTV-Neu mice. This signature will predict the presence of motile cells that will potentially leave the primary lesions and intravasate. We found that E-Cad^{hi} ducts or individual early cancer cells within each duct were more frequently (>60%) P-ATF2^{hi} (**See Appendix**). Accordingly, >85% of HER2+ cells were E-cad^{lo} suggesting that HER2+ cells are more frequently E-Cadlo/P-ATF2lo (**See Appendix**). Complete loss of E-cadherin signal was also observed in HER2+ microinvading MMTV-HER2 early cancer cells in vivo (**See Appendix**). Overt MMTV-HER2 tumors (in FvB mice) showed low levels of E-cadherin, P-p38 and P-ATF2, while maintaining high P-ERK1/2 levels (**See Appendix**), suggesting that a HER2+/P-p38lo/E-cadlo profile is also present in primary tumors. When correlating these markers with HER2 status in human DCIS lesions, an early cancer lesion that is defined as non-invasive, we found that only HER2negative lesions retained both high P-ATF2 levels and organized E-Cadherin junctions (**See Appendix**). In contrast, HER2+ DCIS lesions were typically low for all markers (**See Appendix**). **Conclusion:** We conclude that a signature of early dissemination markers consisting on HER2^{HI}/p-ATF2^{LO}/E-cadh^{LO} could identify motile early-progressed tumor cells and predict for dissemination.

We next tested whether the presence of macrophages in DCIS lesions could predict dissemination. We received de-identified paraffin embedded DCIS sections from patients that had undergone a bone marrow biopsy to determine their DTC status from Tanja Fehm, University Clinic Duesseldorf, Germany. We stained E-Cadherin and macrophages and found that, similar to MMTV-ErbB2 mice, the presence of intra-epithelial macrophages correlated with the loss of E-Cadherin (**Fig.6A,B**). Our positive predictive criterion was high levels for E-Cadherin and low numbers of intra-epithelial macrophages. This analysis was done blindly and samples were then unblinded by our collaboration partners. We correctly predicted 7 out of 10 patients as being positive for the presence of DTCs, resulting in a positive predictive value of 70% (**Fig.6C**). **Conclusion:** We conclude that while the analysis we did is not significant due to the small sample size (N=20), it is a promising result indicating that analyzing the microenvironment of metastasis might be indicative of early dissemination.

Plans for the next year: Depending on the outcome of the experiments in 1.1 and 1.3, we will revisit samples obtained by Dr. Fehm from Germany and refine our P-TMEM analysis by including endothelial cells. In addition we will not continue to increase the sample size to determine if the initial predictive value for the E-cadherin-lo/macrophage+ profile holds as a strong indicator for early dissemination in humans.

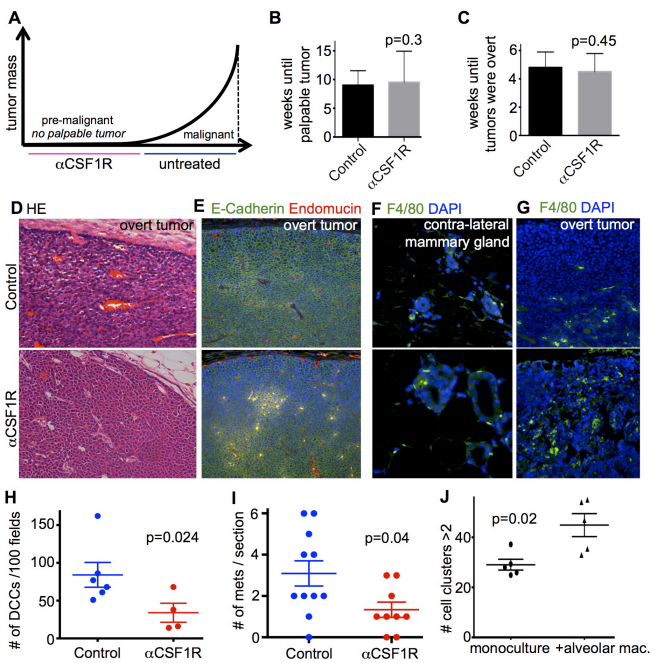

Figure 7. Early disseminated cancer cells can contribute to metastasis formation. Macrophages were depleted by ASF98 treatment in pre-malignant mice starting at week 18 until mice developed palpable tumors (3mm average) and then discontinued (A). Mice were left until tumors reached a diameter of 1cm and then sacrificed. The average time until development of palpable tumors (approximately 3mm in diameter) did not change when pre-malignant MMTV-HER2 mice were treated with the antibody against CSF1Ra (B) and the time until tumors reached a diameter of 1cm was not affected by prior anti CSF1Ra therapy either (C). HE staining (D) and staining against E-Cadherin and Endomucin (endothelial cells; E) in sections of invasive tumors that had been treated with an antibody against CSF1Ra during pre-malignant stages shows no difference to control treated animals. Immunofluorescent staining against F4/80 (F) of contra-lateral mammary gland in animals with overt tumors as well as of invasive tumors (G) showed that CSF1Ra treatment during pre-malignant stages only did not affect mammary tissue or tumor associated macrophage content after cessation of therapy. Solitary DCCs in lung sections (E) and metastases defined as cell clusters bigger than 3 cells (F) were quantified in lung sections stained against for ErbB2.

SA2.1. To test the role of S-TMEM in regulating early DTC dormancy.

Objective: Objectives: 1)- test whether early DTCs assemble S-TMEM for dormancy escape and 2)- expression profile early and late lung DTCs. In this first year majority of the effort was dedicated to Aim 1, which is very advanced in progress. Aim 2.2 showed progress as we need to be able to optimize the DTC isolation as mentioned in section SA1.2, and the optimization of these protocols is underway. Aim 2.1 requires that we validate the components of the TMEM in the lung and this depends on the triple staining that is being optimized in the MMTV-Neu-CFP model and will be finished before the end of 2015. However to further justify the imaging of the S-TMEM function we performed key functional experiments that know provide proof for the functional contribution of macrophages to early DTC fueled metastasis.

2.1 *To test whether early DTCs form S-TMEM and if these influence escape from dormancy.*

Results: We hypothesized that the formation of a S-TMEM is required for the escape from dormancy and that early DTCs might be less efficient to form a S-TMEM. In fact we had shown as preliminary data that DTCs that are not in contact with macrophages are commonly quiescent (P-Rb-), while DTCs (1-10 cell clusters) in contact with macrophages were proliferative (P-Rb+) (not shown). To address the question whether early DTCs influence contribute to the development of metastatic disease, we blocked CSF-1Rα during early and asymptomatic stages of cancer in MMTV-ErbB2 mice, starting at age week 18, and stopped as soon as tumors became palpable. Then we waited until tumors reached 1 cm in diameter (4-6 weeks later) and quantified DTC and metastatic lesion burden (**Fig.7.1A)**. We found that the time to tumor detection as well as the time it took until these tumors were overt was not affected by CSF-1Rα blockade during early cancer stages (**Fig.7B,C**). Additionally, histologic features and macrophage content in contra-lateral mammary glands as well as the invasive tumors and vascularization of tumors at the end of the experiment were comparable in control and in anti- CSF-1Rα treated mice (**Fig.7D-G**). However, CSF-1Rα blockade during early stages of cancer had a profound effect on DTC burden (**Fig.7H**) and late metastasis development (**Fig.7I**) even after macrophage depletion had been stopped for one month in average and animals had carried fast-growing and large invasive tumors. The number of solitary DTCs in late stage animals, likely to be a mixture of DTCs

accumulated since the early stages, was reduced by CSF-1Rα blockade during early stages of cancer. This suggests that the reduced influx of DTCs to lungs during early stages was not replaced by DTCs arriving during the time of tumor detection to euthanasia, a period where large tumors with invasive phenotype grew. Importantly, metachronous micro-metastases were reduced when macrophages had been depleted during early cancer stages.

Conclusions: We interpret that early dissemination, allow for the early target organ colonization by a sub-population of eDTCs that have metastasis initiating capacity or aid the formation of metastatic breast cancer by DTCs that arrive later during progression. The reduction in metastasis can be an aggregate effect of reduced dissemination and also the lack of macrophages or alteration of macrophage phenotype in the lung that could then be unable to stimulate exit from dormancy.

To address whether interaction of DTCs with alveolar macrophages possibly during S-TMEM formation, influences tumor cell proliferation, we performed in vitro experiments, where single 4T1-GFP breast cancer cells were seeded in matrigel (to mimic single DTC biology) either as monocultures or in co-culture with macrophages isolated from BalbC wild type lungs. We found that the presence of alveolar macrophages significantly enhanced the number of 4T1-GFP cells that had grown into small clusters of 2 or more cells (**Fig.7J**).

Conclusion: These data provide further support to the notion that lung macrophages can activate in DTCs metastasis initiating capacity and that the interaction with macrophages as part of a S-TMEM may influence the fate of these DTCs.

Plans for the coming year: Once we confirm by histology the presence of the TMEM structure in lungs we will initiate the imaging of lungs of MMTV-PyMT-ECFP-c-fms-GFP mice while inhibiting p38 signaling as proposed.

2.2 Molecular profiling of early DTCs. In order to recover early and late DTCs in target organs and identify the gene programs distinguishing their behavior we are developing the optimization protocols described for the isolation of CTCs from MMTV-Neu-CFP mice. As indicated we experienced problems due to leakiness of the MMTV promoter in target organs (see SA1.2). However, we anticipate that our alternatives will provide a successful approach to isolate and expression profile these cells.

Plans for the next year: We plan to 1) use an antibody based sorting approach to detect HER2 in CFP+ DTCs and then proceed with the original plan of profiling these cells, and 2) in parallel optimize the detection of DTCs using single cell profiling via HER2 detection and thus have a molecular-based sorting at the single cell level that will then allow detecting the expression profiles in those cells..

Key Research Accomplishment

Specific Aim 1

- Design of a flat window device that allows the imaging of pre-malignant lesions in the tissue fat pad of MMTV-Neu-CFP mouse model.
- Inhibition of p38α/β *in vivo* showed increased motility of pre-malignant MMTV-Neu-CFP cells.
- Identification of a signature consisting on $HER2^{HI}$/p-$ATF2^{LO}$/E-$cadh^{LO}$ that marks motile early-progressed tumor cells and predicts for dissemination.
- Validation of the P-TMEM structure in the MMTV-Neu-CFP mouse model.
- Detection and identification of macrophage subtype linked to early dissemination (Tie2+/VCAM-/CD206+ mammary tissue macrophages)
- Detection of intraepithelial macrophages predicts dissemination in DCIS samples.
- Macrophages in early lesions induce an EMT and promote early dissemination.
- Optimization of a FACS protocol to identify DTCs and CTCs based on double signals for HER2 and CFP (ongoing and this optimization should be counted towards progress in SA2 as well ad it is a technology shared by both aims).

Specific Aim 2

- We optimized a protocol where we blocked CSF-1Rα during early and asymptomatic stages of cancer in MMTV-ErbB2 mice.
- We found that the time to tumor detection as well as the time it took until these tumors to reach was not affected by CSF-1Rα blockade during early cancer stages.
- Histologic features, macrophage content in contra-lateral mammary glands and vascularization of tumors were comparable in control and in anti- CSF-1Rα treated mice.
- CSF-1Rα blockade during early stages of cancer had a profound inhibitory effect on DTC burden in lungs.
- Metachronous micro-metastases were reduced when macrophages were depleted during early cancer stages using CSF-1Rα blockade.
- Lung alveolar macrophages significantly enhanced the number of 4T1-GFP cells that transitioned from single solitary cell state to proliferative small clusters, mimicking reactivation from dormancy.

Reportable Outcomes:
Publications relevant to this project:

Publications:

1. Goossens N, Hoshida Y, **Aguirre-Ghiso JA**. Origin and interpretation of cancer transcriptome profiling: the essential role of the stroma in determining prognosis and drug resistance. ***EMBO Mol Med. 2015*** Aug 3. pii: e201505284. doi: 10.15252/emmm.201505284. [Epub ahead of print] No abstract available.

Manuscripts Submitted:

1. Kathryn Harper*, Maria Soledad Sosa#*, Hedayatollah Hosseini, Alvaro Avivar Valderas, Chandandaneep Nagi, Roger Davis, Christoph Klein, David Entenberg, John Condeelis, Eduardo F. Farias and Julio A. Aguirre-Ghiso#. "Identification of an ErbB2+ early disseminating pre-malignant cancer cell sub-population with metastatic potential". *denotes equal contribution. # denotes corresponding authors. Under review in ***Cancer Cell.***

2. Hedayatollah Hosseini, Kathryn Harper, Maria Soledad Sosa, Lahiri Kanth Nanduri, Christian Werno, Carolin Ehrl, Matthias Maneck, Milan Obradovic, Nina Patwary, Gundula Haunschild, Christian Reimelt, Florian Weber, Josef Schroeder, Julio Aguirre-Ghiso, Piero Musiani, Andreas Hartkopf, Florin-Andrei Taran, Tanja Fehm, Gunter Meister, Christoph A. Klein. "Her2 and progesterone signaling cooperate for early dissemination of breast cancer cells". Under review in ***Cancer Cell***

Oral presentations:

- **2014: Speaker at the ACTC**, October 8-11 2014, Crete, Greece
- **2014: Speaker at the Washington University School of Medicine**, November 5 2014, St Louis, MD
- **2014: Speaker at the 2014 ASCB/IFCB meeting,** December 6-10 2014
- **2015: Speaker, TMEN Steering Committee Meeting,** 21-23 January 2015. Seattle, WA
- **2015: Keynote Speaker – Porto Cancer and Stem Cells meeting, IPATIMUP,** Porto, Portugal.
- **2015: Speaker – FASEB Summer research Conference on TGFβ signaling,** Snowmass CO, USA.
- **2015: Speaker – University of Colorado Cancer Center,** Denver CO, USA.
- **2015: Speaker – University of Kentucky,** Lexington**,** KY, USA.
- **2015: Speaker – Samuel Waxman Cancer Research Foundation Annual Symposium**, Mount Sinai School of Medicine, New York, NY, USA.
- **2015: Speaker – Weill Cornell College of Medicine,** New York, NY, USA

Posters
Several poster presentations from lab members. Can be provided upon request.

Awards
NA

CONCLUSION

SUMMARY OF FINDINGS:

Progress in our first year of funding has been highly significant as we have detected all components of TMEM structures during early dissemination, proven the function of TMEM components such as mammary tissue macrophages in the early dissemination of HER2+/E-cad^{lo}/P-p38/PATF2^{lo} early cancer cells and we also tested their contribution to metastasis. Importantly we provide an identity for the MTMs as they show a Tie2+/VCAM-/CD206+ profile. We also found that early-progressed cancer cells undergo an EMT program that via intrinsic and extrinsic pathways endow them with motile capacity and dissemination to secondary organs. We identified an early dissemination signature that includes HER2^{HI}/p-ATF2^{LO}/E-cadh^{LO} and marks motile early-progressed cancer cells with potential to disseminate. Moreover, this signature when combined with the macrophage+ detection in DCIS samples, correlated with the presence of bone marrow DTCs in 70% of cases that patients had disseminated disease. Overall, our findings support our hypothesis that early dissemination contributes to metastasis but also to a dormant DTC population that may be reactivated from dormancy by macrophages in the lung. Our knowledge on DTCs behavior and their interactions with the microenvironment is limited. Our identification of the origins of DTCs may help to understand their biology and how to suppress dissemination to avoid metastasis formation.

SIGNIFICANCE:

Our work is revealing an unexpected contribution of early DTCs to dormancy and metastasis in cooperation with macrophages. This argues that we need to better understand the disseminated disease to better manage metastatic progression. Our work provides a new biology to develop novel therapeutic strategies. This is more relevant because we also have a clear component of human cancer analysis in our proposal that is already providing insights. Our work is very relevant as there is great confusion on how to treat women with stage 0 breast cancer. A recent study published in JAMA Oncology adds to this confusion as it shows that while breast cancer deaths from DCIS metastasis are ~3% of the whole population, 50% (thousands of women each year) die of metastasis in the absence of an invasive breast cancer recurrence and the choice of therapy did not affect survival. This suggests that the DTCs remain untouched by therapies and that, a subpopulation of women with stage 0 breast cancer carry early disseminated cancer cells that can have deadly consequences. We therefore need better tools to identify those stage 0 patients at high risk of developing late metastatic relapses without over treating the majority of women who have harmless variants of DCIS. Interestingly, our collaboration with Dr. Fehm and Dr. Karn from Germany, is allowing us to show that those women with DCIS who carry disseminated tumor cells in their bone marrow often had a E-Cadherin low/macrophage high signature. This may serve as a predictive tool if validated.

References:

1. Rohan, T.E. *et al.* Tumor microenvironment of metastasis and risk of distant metastasis of breast cancer. *J Natl Cancer Inst* **106** (2014).
2. Wen, H.C. *et al.* p38alpha Signaling Induces Anoikis and Lumen Formation During Mammary Morphogenesis. *Science signaling* **4**, ra34 (2011).
3. Entenberg, D. *et al.* Setup and use of a two-laser multiphoton microscope for multichannel intravital fluorescence imaging. *Nature protocols* **6**, 1500-1520 (2011).
4. Harney, A.S. *et al.* Real-Time Imaging Reveals Local, Transient Vascular Permeability, and Tumor Cell Intravasation Stimulated by TIE2hi Macrophage-Derived VEGFA. *Cancer discovery* **5**, 932-943 (2015).
5. Franklin, R.A. *et al.* The cellular and molecular origin of tumor-associated macrophages. *Science* **344**, 921-925 (2014).

Appendix 1: Manuscript for:

Kathryn Harper*, Maria Soledad Sosa#*, Hedayatollah Hosseini, Alvaro Avivar Valderas, Chandandaneep Nagi, Roger Davis, Christoph Klein, David Entenberg, John Condeelis, Eduardo F. Farias and **Julio A. Aguirre-Ghiso#**. “Identification of an ErbB2+ early disseminating pre-malignant cancer cell sub-population with metastatic potential”. *denotes equal contribution. # denotes corresponding authors. Under review in ***Cancer Cell.***

Mechanism of early dissemination and metastasis during early stages of HER2+ mammary cancer.

Kathryn L. Harper[1#], Maria Soledad Sosa[1#*], Hedayatollah Hosseini[2], David Entenberg[4], Alvaro Avivar- Valderas[1], Chandandaneep Nagi[1], Roger J. Davis[3], Eduardo F. Farias[1], John Condeelis[4], Christoph Klein[2], and Julio A. Aguirre-Ghiso[1*]

[1]Division of Hematology and Oncology, Department of Medicine, Department of Otolaryngology, Department of Oncological Sciences, Tisch Cancer Institute, Black Family Stem Cell Institute, Mount Sinai School of Medicine, New York, NY 10029, USA. [2]Experimental Medicine and Therapy Research Faculty of Medicine University of Regensburg, 93053 Regensburg, Germany. [3]Howard Hughes Medical Institute, University of Massachusetts Medical School, MA 01605, USA. [4]Department of Anatomy and Structural Biology, Integrated Imaging Program, Gruss Lipper Biophotonics Center, Albert Einstein College of Medicine, 1300 Morris Park Ave, Bronx, NY 10461, USA.

[*]*Correspondence to:* Maria Soledad Sosa and Julio A. Aguirre-Ghiso, Division of Hematology and Oncology, Department of Medicine, Head and Neck Cancer Research Program, Department of Otolaryngology, Mount Sinai School of Medicine, New York, NY, 10029. Phone: 212-241-9582 Fax: 212-241-4096 Box: 1079 E-mails: maria.sosa@mssm.edu, julio.aguirre-ghiso@mssm.edu

# Denotes equal contribution.

Running title: Signaling pathways regulating early dissemination

SUMMARY

The mechanisms that produce early-disseminated cancer cells (eDCC) during early stages of breast cancer are poorly understood. Here we show that during early mammary cancer, when only ADH or DCIS lesions are present, there is a sub-population of HER2+ early cancer cells that are invasive and highly efficient in disseminating to target organs. These eDCC were HER2^{+}/P-ATF2^{lo}/E-cadherin^{lo}, and were found also in human DCIS samples. Further, eDCCs underwent a Wnt-dependent EMT-like response that was reversed by HER2 or Wnt signaling blockade. Intra-vital imaging of transgenic HER2-CFP early lesions revealed that eDCC precursors locally invade, intravasate and circulate to target organs. Surprisingly, although the vast majority of eDCCs are non-proliferative, they can still initiate metastasis. We conclude that during stages of cancer considered broadly non-invasive, some HER2+ cancer cells can aberrantly activate an invasive morphogenetic program causing early dissemination. These eDCCs carry latent metastatic initiating capacity, which impacts our understanding of metastasis onset and how it might be targeted effectively.

INTRODUCTION

Metastasis is the leading cause of breast cancer (BrCa) related deaths and can often occur after prolonged periods of latency (>20 years), possibly due to the existence of quiescent/dormant disseminated cancer cells (DCC) (Klein, 2010; Sosa et al., 2014). Active and dormant DCCs may contribute to the phenotypic and genetic heterogeneity of metastasis initiating cells and therapy failure (Husemann et al., 2008; Sosa et al., 2014). However, the source of DCCs contributing to this heterogeneity is not fully known and central to preventing metastasis related deaths.

More importantly, during what point in cancer evolution do DCCs originate and fuel metastasis has remained a key question. Solid evidence supports that micro-invading cells and eDCCs are detected in BrCa patients diagnosed with lesions pathologically defined as pre-invasive (i.e. ductal carcinoma in situ DCIS)(Husemann et al., 2008; Schardt et al., 2005). This suggests that DCCs may originate long before tumors are detectable or are defined globally as “invasive” by a pathologist. However, the signals that limit or activate the programs that could fuel early dissemination are unknown.

Anoikis resistance is a trait of metastatic cells needed to negotiate stress imposed by the varying composition of extracellular matrix microenvironments and loss of adhesion in circulation. Interestingly, anoikis resistance is activated at early stages of HER2-driven mammary cancer by inhibiting the p38 kinase, known to also suppress breast tumorigenesis (Bulavin et al., 2002; Ventura et al., 2007; Wen et al., 2011). This process is also accompanied by ERK1/2 activation, which positively regulates motility and invasion (Klemke et al., 1997; Pearson and Hunter, 2007), and changes in the ductal architecture. Importantly, inactivating mutations in the p38 activator MKK4 (Su et al., 2002; Teng et al., 1997) and amplification of the p38 phosphatase PPM1D (Bulavin et al., 2002; Bulavin et al., 2004b) are also frequent in breast cancer, suggesting that different mechanisms might allow for inactivation of p38–induced anoikis among other processes. We hypothesized that inhibition

of p38 signaling might allow anoikis resistant HER2+ early cancer cells to acquire motility programs that enable dissemination to distant organs.

Here we show that HER2 overexpression results in the activation and inhibition of Wnt and p38 signaling, respectively, and in the induction of an EMT-like program similar to that observed during mammary gland morphogenesis (Brisken et al., 2000; Nelson et al., 2006; Wen et al., 2011). In early $HER2^{+}$ cancer cells p38α/β inhibition further induces the Wnt-driven EMT dramatically stimulating local invasion and early dissemination to target organs, as revealed by live high-resolution imaging. This coincides with the time at which dissemination is more pronounced (see accompanying manuscript by Hosseini et al.). Surprisingly, MMTV-HER2+ early cancer cells, while non-tumorigenic in primary sites, could activate lung metastasis initiating programs after variable time periods. Our work reveals a previously unrecognized molecular mechanism for early dissemination where morphogenesis programs like those regulated during mammary ductal tree development (Brisken et al., 2000; Nelson et al., 2006; Wen et al., 2011) may be subverted early during cancer progression to foster early dissemination and spawn numerous eDCCs with metastasis-initiating capacity.

RESULTS

Tumorigenic and Metastasis Initiating capacity of early HER2+ cancer cells.

eDCCs can be detected in the bone marrow (BM) during pathologically defined pre-invasive stages of breast cancer (i.e.DCIS) in both patients and in the Balb-C-derived Balb-Neu-T (NeuT active mutant, MMTV-Her2-T **S-Fig1E**) and MMTV-PyMT mouse models of breast cancer (Husemann et al., 2008; Schardt et al., 2005). Interestingly, it is during this time and not during the time when primary tumors are overt, that dissemination is maximal (see Hosseini et al.). Using the FvB-derived MMTV-HER2(wt) model (Wen et al., 2011) (**S-Fig1E)**, we detected eDCCs in lungs or BM during stages where gross pathological analysis reveals only early lesions (ADH,DCIS) and no primary tumors are detected. Disseminated cancer cells detected in animals bearing overt tumors

were named DCCs because they represent a mixture of eDCCs and those that arrived later. We found that HER2+/CK8/18+ eDCCs are detected in the blood, BM and lungs of 100% of 14-18 weeks old mice, when only early lesions and no tumors are present (**Fig1A-C, S-Fig1A;** note that the time courses of the FvB-derived and BALB/c-derived MMTV-HER2 (Balb-NeuT) models differ). Thus, early dissemination is commonplace in different models of breast cancer.

To characterize the behavior of DCCs in lungs we detected P-Rb levels, a marker of G1-exit, in HER2+ single cells (1-3 cell clusters) during early (14-18 weeks) or overt primary tumor stages (28 weeks), where a mixture of single DCCs, micro- (3-50 HER2+ cells) and macro-metastasis (>50 HER2+ cells) is observed (**Fig. 1 D&G, S-Fig1B**). In lungs of mice bearing only early lesions we rarely found micro or macrometastasis and eDCCs predominated as single cells or small clusters (2-3 cells, **Fig. 1 D&G, S-Fig1B**). We found that the vast majority of solitary eDCCs (1-3 cells) in lungs during early stages were negative or weakly stained for P-Rb (19% P-Rb^{weak,} 0% P-Rb^{strong}) compared to growing micro and macro-metastases in mice carrying overt lung lesions and primary tumors (80% P-Rb^{strong}) (**Fig1D&G**). In animals with overt tumors solitary DCCs (1-3 cells) became more proliferative as measured by P-Rb fluorescence intensity (**Fig1D, data not shown**) but even lungs bearing proliferative micro- and macro-metastases (28 weeks old) had numerous quiescent P-Rb^{negative} HER2+ DCCs (**Fig1D&G**). We conclude that early DCCs are a population of primarily P-Rb^{negative} cancer cells and that even in animals bearing metastases >50% of single or small groups of DCCs (2-3 cells), which likely are a mixture of early and later arriving DCCs, are non-proliferative or slow cycling.

We next prepared spheres from early stage MMTV-HER2 cells (**S-Fig1C**) or tumorspheres from overt MMTV-HER2 tumors. After orthotopic injection in nude mouse mammary fat pads, tumorspheres (~300/site) from overt tumors efficiently formed primary tumors within 4-12 weeks (**Fig 1E**). However, HER2+ mammospheres (~300/site) produced no palpable tumors in this time (**Fig 1E**). Surprisingly, with an incidence of ~21% (n=14), animals injected with HER2+ mammospheres developed lung metastases (overt and micrometastases) (**Fig. 1E-F**). Macro-metastases from early

cancer cells contained in the mammospheres displayed a glandular phenotype but also an undifferentiated morphology (**Fig1F**). Micrometastases also displayed cortical HER2+ staining and were P-Rb^{strong} (**Fig1F**). Further, macro-metastases originating spontaneously in autochthonous MMTV-HER2 mice had a similar percentage of P-Rb^{strong} tumor cells to those derived from mammospheres (**Fig1F-G**). While we were able to detect single DTCs in tumorsphere injected mice we were unable to find macro-metastases (**Fig 1E, S-Fig1D**). This suggests that metastases originating from early cancer cells contained in the mammospheres once they initiate growth they proliferate at similar rates as those originating in mice with large primary tumors. We conclude that early HER2+ mammospheres activate powerful programs of dissemination (motility+invasion), while tumorspheres seem to be predominantly committed to a proliferation program and less to dissemination. However, eDCCs derived from early HER2+ mammospheres are able to survive and activate metastasis-initiating programs (**Fig1E&F**).

HER2^{+}/E-cad^{lo}/P-p38^{lo} early Cancer Cells are Motile and Invasive.

We published that inhibition of MKK3/6-p38α/β signaling in wt or early stage HER2+ lesions resulted in anoikis resistance and intermixing of myoepithelial and epithelial cells suggestive of motility (Wen et al., 2011). Thus, we tested whether the combined loss of p38 signaling and upregulation of HER2 in early cancer cells might activate a disseminating phenotype.

Detection of P-ATF2 (a p38 activity readout - (Wen et al., 2011)) and E-cadherin (epithelial marker) in HER2+ and HER2-T+ (from Balb-NeuT) tissues at early stages of progression showed great inter-ductal and intra-ductal heterogeneity of expression (**Fig2A**). We found that E-Cad^{hi} ducts or individual early cancer cells within each duct were more frequently (>60%) P-ATF2^{hi} (**Fig2A**). Accordingly, >85% of HER2^{+} cells were E-cad^{lo} suggesting that HER2^{+} cells are more frequently E-Cad^{lo}/P-ATF2^{lo} (**Fig2B**). Overt MMTV-HER2 tumors (in FvB mice) showed low levels of E-cadherin, P-p38 and P-ATF2, while maintaining high P-ERK1/2 levels (**Fig2D, S-Fig2A**), suggesting that a HER2^{+}/P-p38^{lo}/E-cad^{lo} profile is also present in primary tumors. When correlating these markers with

HER2 status in human DCIS lesions, an early cancer lesion that is defined as non-ivasive, we found that only HER2^{negative} lesions retained both high P-ATF2 levels and organized E-Cadherin junctions (**Fig2C, S-Fig 2B**). In contrast, HER2^{+} DCIS lesions were typically low for all markers (**Fig2C, S-Fig2B**). As in the MMTV-HER2 mouse model (**Fig2A**), the P-p38/P-ATF2^{lo} profile appears to be present also in HER2^{+} invasive breast carcinomas (n=20) where only HER2^{negative} tumors showed very strong nuclear staining for P-p38 and P-ATF2 (**Fig2E and S-Fig2C)**. HER2 activation inhibited p38 signaling and E-cadherin junction formation, because treatment of HER2-MCF10A cells, which overexpress HER2, with lapatinib (100 nM, 24 hrs) restored E-cadherin junctions and P-ATF2 levels (**Fig2F**). EGFR, expressed in MCF10A cells, does not appear to play a role in E-cadherin and P-p38 downregulation as these cells which are grown in the presence of EGF retain in basal conditions E-cadherin junctions and high p38 activation (Debnath et al., 2002; Wen et al., 2011). Thus, lapatinib at these doses does not seem to have noticeable off target effects. HER2-expressing MCF10A or early MMTV-HER2 cells also resisted anoikis in 3D organotypic cultures and formed misshapen lumen-filled acinar structures as reported (**Fig3A&3C**). These aberrant acini showed outward micro-invasion of single cells (**Fig3A, C, D**) rich in f-actin decorated invadopodia, loss of E-cadherin and focalized laminin-V degradation (**Fig3A, C, D**). Complete loss of E-cadherin signal was also observed in HER2^{+} microinvading MMTV-HER2 early cancer cells *in vivo* (**Fig3B**). Interestingly, ~80% of microinvading cells were HER2^{+} and CK8/18^{+}, suggesting that downregulation of E-cadherin does not indicate a complete loss of epithelial identity; only 20% of CK8/18+ microinvading cells were negative for HER2, which might represent a highly migratory subpopulation identified *in vitro* by Hosseini et al (**S-Fig2D**). The downregulation of E-cadherin in HER2^{+} cells was vigorously stimulated in isolated early HER2+ cancer cells and in the MCF-10A-HER2 model by further forcing an HER2^{+}/p38^{lo} profile using p38α siRNA or the p38α/β inhibitor (SB203580) (**Fig3C, D** & **Fig4A-B**). In 3D cultures, occasionally we could observe what appeared to be collective invasion and only after p38α/β inhibition (**Fig3C and D**). We conclude that a subpopulation of HER2^{+}/E-cad^{lo}/P-ATF2^{lo}/P-p38^{lo}/CK8/18+ early invasive cancer

cells are at early stages of cancer progression and that HER2 signaling actively induces a P-p38^{lo}/E-cad^{lo} profile.

Early HER2^{+}/P-p38^{lo} cancer cells display characteristics of an EMT.

The loss of E-cadherin junctions led us to test whether a HER2^{+}/P-p38^{lo} profile was linked to the partial or total activation of an epithelium to mesenchyme transition program (Thiery et al., 2009). Treatment of MCF10A-HER2 acini with a p38α/β inhibitor SB203580 or siRNAs targeting p38α or ATF2 (**Figs3-4**), further accentuated the invasive behavior and caused a dramatic loss of E-cadherin junctions (**Fig4A-B**). A similar effect was found in early MMTV-HER2 cells freshly isolated from mice (16 wks) (**Fig4B, S-Fig 1D**). We also found that both genetic and pharmacological inhibition of p38α or p38α/β, respectively reduced membrane-bound β-catenin and increased active-β-catenin (unphosphorylated β-catenin) (**Fig4A-B**). Accordingly, in early stage MMTV-HER2 glands we found ~66% HER2^{+} cancer cells to be low for membrane localized β-catenin (indicating pathway activation) (**Fig4D, S-Fig 3A**). Activation of β-catenin signaling in HER2^{+} cells by p38α/β inhibition was confirmed by upregulation of Axin2 mRNA (a canonical target of β-catenin) in MCF10-HER2 cells (**Fig4C**). The intraductal heterogeneity of HER2 overexpression and membrane β-catenin was observed in both MMTV-HER2 and Balb-NeuT models (**Fig4D, S-Fig3A**). In fact, in >70% of early cancer cells that were HER2^{+} were also low for membrane β-catenin (**Fig4D, S-Fig3A**). Quantification of E-Cadherin expression showed that the vast majority of HER2+ eDCCs (1-3 cell clusters) in lungs were negative for E-cadherin (**Fig4E**). This argues that the loss of E-cadherin possibly activated by the EMT-like response, persists in the single eDCCs (1-3 cell clusters) in lungs (**Fig1**).

Importantly, systemic inhibition of p38α/β for 2 weeks in MMTV-HER2 mice at early stages of progression (14-18 wks old) when no palpable tumors are detectable (**S-Fig 1D**), caused a robust translocation of β-catenin from the membrane to the nucleus and a dramatic loss of E-cadherin junctions in the vast majority of early cancer cells (**Fig5A-B**). Thus, a certain level of p38α/β activity

might represses an EMT-like phenotype and prevent HER2$^+$ early cancer cells from disseminating. To confirm this prediction we measured CK8/18+ and/or HER2+ pre-malignant cancer cells in peripheral blood, in BM and lungs of MMTV-HER2 mice carrying early lesions (**Fig5C-E**). We found that a 2 week treatment with SB203580 robustly increased the numbers of CK8/18+ circulating cancer cells. This was followed by an increase in the total number of CK8/18+/HER2$^+$ eDCCs in the BM and HER2$^+$ eDCC in lungs (**Fig5C-E**). The detection of CK8/18 alone or with HER2 in BM eDCCs argues that these are epithelial cells and not leukocytes with ectopic expression of HER2 due to MMTV aberrant activation as reported previously (Husemann et al., 2008). The median number of eDCCs in the BM compartment is equivalent to ~1.3 eDCCs/ 10^6 BM host cells in control groups and ~8 eDCCs/10^6 BM host cells in SB203580 treated animals. We did find that some eDCCs were CK8/18+ and HER2-negative as found by Hosseini et al. (not shown), suggesting that both subpopulations may be disseminating individually or in a cooperative manner. However, only when considering the HER2$^+$/CK8/18+ early DCCs the stimulation of dissemination by SB203580 was significant; HER2 might enable a more efficient EMT-like response to p38 inhibition (**Fig5C-E**). These data confirm that early HER2$^+$ cancer cells disseminate and can be further stimulated to exit the early lesions by forcing a p38^{lo} profile.

To test the contribution of p38 to the EMT-like behavior independently of HER2, we compared E-cadherin junctions and membrane/nuclear β-catenin in wild type FvB mice treated with or without SB203580 or wild type MKK3+/+|MKK6+/+ and MKK3−/−|MKK6+/− C57B mice (MKK3 and MKK6 activate all p38 isoforms). We found that in normal wild type tissues, inhibition of the MKK3/MKK6-p38 pathway caused a loss of E-cadherin junctions (**S-Fig3G**), but not nuclear translocation of β-catenin (**S-Fig3H**). Further, the mammary duct architecture was not perturbed despite the loss of E-cadherin junctions because luminal cells expressed CK8/18 and the α-smooth muscle actin positive myoepithelial layer was intact (**S-Fig3H**). We conclude that SB203580 recapitulates the genetic ablation of the MKK3/MKK6-p38 pathway and that this pathway regulates E-Cadherin junction

formation (**S-Fig3G**). Further, only in the context of HER2 upregulation does p38 inhibition induce nuclear translocation of β-catenin (**Fig5A-B**).

High-resolution live-cell imaging of early dissemination.

We next used high-resolution intra-vital imaging (Entenberg et al., 2011) of MMTV-HER2-CFP transgenic mice to unambiguously record at single-cell level resolution the micro-invasive capacity of early $HER2^+$ invasive cancer cells (**Fig6, S-Fig1E**). To monitor early cancer cell motility before primary tumor development we designed a mammary imaging window to accommodate the depth and lax consistency of the mammary fat pad tissue. 2-photon imaging of a small fraction of the ductal tree in vehicle treated HER2-CFP mice where the vasculature is revealed by i.v. delivered dextran-rhodamine (DR) (Entenberg et al., 2011)) showed that early cancer cell motility and local invasion was infrequent at 10 weeks when the ducts in the MMTV-HER2-NDL5-CFP model still display normal ductal architecture (**Fig6A – Supplemental Movie 1)**. However, at 15 and 18 weeks of progression when early lesions are observed (**Supplemental Fig1**), local invasive CFP+ cell translocation and cell motility were detectable even in an imaging area that captures a very small fraction of the transgenic mammary tree (**Fig6A - Supplemental Movies 2 and 3**). At this time we could also detect CFP+ cell translocation and exit from lesions into the stroma (**Fig6A - Supplemental Movies 2 and 3**). Forcing a $HER2^+$/E-cad^{lo}/P-$p38^{lo}$ profile using a p38α/β inhibitor revealed a strong disruption of the ductal architecture (compare **Fig6A, "normal" architecture, with Fig6B-D and Supplemental Movie 1 with 4**); control ducts at week 12 look similar to those at week 10 in **Fig6A**.

Importantly, p38α/β inhibition revealed at high-resolution active formation of cell protrusions, intra-ductal migration, locomotion along ductal walls and local invasion and intravasation (**Fig6B top and sequence below and Supplemental Movie 4 and 5**). Unlike in 3D cultures (**Fig3C-D**), we did not observe obvious collective cell migration *in vivo* and cells displayed more ameboid-like features that may facilitate invasion (Liu et al., 2015). High-resolution imaging and 3D reconstruction of the

micro-invasion and intravasation events showed how individual cells micro-invaded outwards from the ductal pre-malignant lesions and invaded through the stroma (**Fig6D - Supplemental Movies 6, 7 and 8**) entering in contact with the blood vessels (**Fig6D - Supplemental Movie 8 and 9**). These high-resolution intra-vital imaging studies unambiguously document early pre-malignant micro-invasion and intravasation.

HER2^{+}/P-p38^{lo} early cancer cells acquire a Wnt^{hi} phenotype.

We next measured the expression of 86 EMT related genes expressed in control (DMSO) and SB203580 treated MCF10A and MCF10A-HER2 acini (**Fig7A**). HER2 expression or p38 inhibition alone induced a shared 14-gene EMT signature (**Fig7A**), suggesting that both kinases operate antagonistically on the same pathway. The signature, (confirmed by subsequent qPCR (**S-Fig3B-C**)), included non-canonical *WNT* ligands (WNT5a/b, WNT11) and a WNT receptor (*FRZD7*), canonical EMT transcription factors (*TWIST, SNAIL, SLUG*) and *ERBB3* and was further upregulated by p38 inhibition in HER2-MCF10A cells (**Fig7A**). Wnt4 (not in our array) was also upregulated in murine early cancer cells (Hosseini et al.) and *E-cadherin* mRNA was downregulated by p38 inhibition in HER2-MCF10A acini (**Fig7B**). *SNAIL* and *TWIST* were also upregulated when HER2-MCF10A 3D cultures were treated with siRNAs targeting *p38*α or *ATF2* (**S-Fig3D**), and systemic treatment of early MMTV-HER2 mice with SB203580 resulted in an 8-fold upregulation in *TWIST*, mRNA in mammary gland tissues *in vivo* (**Fig7B**). These data suggest that p38 exerts an inhibitory function over HER2 signaling and Wnt-ligand expression in early cancer cells and confirm that *in vivo* p38 signaling restricts the expression (*TWIST)* and/or function (β-catenin) of EMT transcription factors. We conclude that HER2 activation and p38 inhibition cooperate to establish a Wnt signaling-associated EMT, which is sufficient to allow early invasive cancer cells to disseminate.

We next tested if Wnt ligands (**Fig7A and S-Fig3B&C**) were playing a functional role in HER2-driven EMT either alone or in combination with p38 inhibition. When HER2-MCF10A cells were

treated with SB203580 the *Axin2* (β-catenin target – canonical Wnt signaling) mRNA was induced and this response was almost completely eliminated in MCF10A-HER2 cells expressing the Wnt-ligand antagonist sFRP (canonical and non-canonical Wnt ligand inhibitor) (**Fig7C, S-Fig3E**). Recombinant soluble Wnt3a produced by L-cells ((Grumolato et al., 2010) and methods) also stimulated expression of *Axin2* in HER2-MCF10A cells. Importantly, Wnt3a induction of *Axin2* was significantly inhibited by overexpression of a constitutively active p38α □□□□□□ cDNA (**Fig7D**). We conclude that $HER2^{+}/p38^{lo}$ pre-malignant cells rely on Wnt ligands, possibly both canonical and non-canonical, to induce the EMT.

Next, HER2-MCF10A and sFRP expressing HER2-MCF10A cells were treated with or without SB203580 (**Fig7E-F, S-Fig 3E**). Loss of E-cadherin junctions and membrane-localized β-catenin after p38α/β inhibition was blocked in sFRP expressing cells (**Fig7F**). Importantly, the micro-invasion that observed in $HER2^{+}/P\text{-}p38^{lo}$ colonies after p38 inhibition, was blocked by sFRP (**Fig7E-F**) and by the canonical Wnt inhibitor DKK1, which also reversed the E-cadherin loss induced by p38 inhibition (**S-Fig 3F**). Our data and the finding that in the Balb-NeuT model (Hosseini et al.), Wnt4 and RANKL upregulation promote a highly migratory signal in early cancer cells led us to conclude that *via* Wnt signaling HER2 activation in the context of low p38α/β activity results in an EMT-like response. Collectively these signals allow a previously identified (Husemann et al., 2008) but not characterized (include Husseman et al.) sub-population of early invasive cancer cells to disseminate.

DISCUSSION

Previous studies determined that early DCCs are present in the MMTV-HER2 model and in patients. These is a subpopulation of cells that, using electron microscopy, were shown to micro-invade and would have likely not been detected by conventional pathological analysis in glands that displayed ADH and DCIS like lesions (Husemann et al., 2008). Our findings now provide a molecular and mechanistic description of these cells by identifying this subpopulation of early invasive cancer

cells as HER2^{+}/CK8/18+/Wnt^{high}/P-p38^{low}/E-cad^{low}. We further show that the eDCC precursors carry an inherent capacity to migrate, intravasate and lodge in secondary organs. Remarkably, these eDCCs show metastasis-initiating capacity. In both our and the Hosseini et al., study, early cancer cells disseminated spontaneously in both MMTV-HER2-wt (FvB-HER2) and –ErbbB2-T (Balb-NeuT) models from autochthonous tissue, fat pad injected mammospheres or from transplanted pre-malignant mammary tissue (Hosseini et al). Thus, eDCCs are able to complete all steps of metastasis. As shown by Hosseini et al., this dissemination seems to be even more efficient than that produced by large primary tumors. A majority of HER2^{+} eDCCs once in lungs are predominantly negative for P-Rb, a marker of proliferation. This suggests that eDCCs can enter a state of dormancy or slow-cycling. As seen following the injection of early cancer cell-derived mammospheres into the fat pad of nude mice, eDCCs eventually were able to form HER2+ metastasis in the absence of overt tumors. That early cancer cell-derived mammospheres did not form primary tumors when injected into the mammary fat pad, suggests that unlike the lung, it is not permissive for growth but is permissive for invasion and dissemination.

We discovered that a balance that favors HER2 and Wnt over E-cadherin and p38 signaling, results in early dissemination by blocking the ability of p38 and E-cadherin to block an EMT-like program. The vast majority (~98%) of eDCCs in lungs, which were also single cells or 2-3 cell clusters, were HER2+ but E-cadherin negative and only a very small fraction appeared to be able to restore E-cadherin expression and this was observed only in clusters. However, the micro-invading cells and a proportion of eDCCs in the bone marrow were CK8/18+, suggesting that a partial EMT program may be sufficient for early dissemination. For example, dissemination proceeds when collective invasion is activated in CK14+/p63+ basal mammary epithelial cells without evidence of EMT (Cheung et al., 2013). Also early cancer cell dissemination may follow a basic program of invasion that does not require an EMT and/or E-cadherin downregulation as shown in mammary epithelial cells (Shamir et al., 2014). Further, changes in the microenvironment that may be imperceptible such as 3D physical space confinement may allow cells to microinvade *via* the

acquisition of an amoeboid movement without the need of altered genomes(Liu et al., 2015). We argue that when HER2 upregulation is combined with p38 inhibition at least a 14-gene EMT signature is activated and this was linked to enhanced dissemination. But HER2 upregulation or p38 inhibition alone were also able to induce this signature albeit less strongly. Thus, it is possible that even these lower signals for EMT coupled to other microenvironmental cues (Liu et al., 2015) cause a less frequent but persistent disseminating phenotype in early invasive cancer cells. That p38 signaling prevents the loss of E-cadherin and turning on an EMT-like program is a novel finding. However, how p38 signaling executes these functions is not entirely clear. ATF2 is a likely candidate in activating a program that prevents an EMT as it can block β-catenin activity (Bhoumik et al., 2008). Accordingly, *ATF2* RNAi upregulated *TWIST and SNAIL* and a constitutively active p38α mutant suppressed *AXIN2* induction by Wnt3a. Our data suggests the EMT program might be maintained in solitary eDCCs in lungs, because these cancer cells were $HER2^{+}$/E-$cadherin^{lo}$ several weeks after dissemination. Thus, in early cancer cells, HER2-driven EMT gene expression might lead to a strong and perhaps long-term mesenchymal-like phenotype that induces single eDCC dormancy, as proposed by others (Brabletz, 2012).

Hosseini et al., found that the gene signature present in early lesions that is associated with early dissemination, was significantly enriched for genes in the p38 and TGFβ pathways. This strengthens the role of these pathways in regulating eDCC egress. Our findings also suggest that Wnt5a, Wnt5b, Wnt11 may be important to induce the EMT as sFRP and DKK1 could restore epithelial identity in human $HER2^{+}$/P-$p38^{lo}$ cells. Hosseini et al., also found that Wnt4 may be important for murine early cancer cell dissemination, further strengthening a Wnt-driven program of dissemination of cancer cells with less evolved genomes. It is important to note that TGFβ and Wnt signaling regulate side branching during mammary gland development (Brisken et al., 2000). Our data suggest that $HER2^{+}$ cells may aberrantly activate a program of motility and invasion observed during branching morphogenesis that requires downregulation of p38 signaling and leads to

dissemination. Interestingly, Wnt and TGFβ signaling in conjunction with progesterone receptor-B (PgR) favored side branching (Brisken et al., 2000). With Hosseini et al., we also found that PgR signaling is enriched in the pre-malignant tissues that spawned eDCCs. As highlighted by Hosseini et al., wild type ducts that were still undergoing morphogenesis showed also a PgR^{hi}/$P\text{-}ATF2^{lo}$ profile. This supports our hypothesis that HER2 co-opts a mechanism of invasion and motility active during morphogenesis (Brisken et al., 2000) and that its deregulation results in early dissemination. Importantly, PgR-signaling is known to induce Wnt4 expression and PgR and HER2 expression only overlapped during early stages of mammary cancer progression in the MMTV-Neu models. Thereafter, PgR expression is lost (Hosseini et al).

Together, the Hosseini et al. and our data support a model where a balance that favors at least oncogenic HER2, PgR and Wnt over E-cadherin and p38 signaling in early stages of breast cancer progression may awaken programs of motility, invasion and stem cell-like behavior observed during pregnancy in the mammary gland. These data also suggest that p38 concomitantly functions as a tumor suppressor by affecting cell cycle and anoikis mechanisms (Bulavin et al., 2002; Bulavin and Fornace, 2004a; Maekawa et al., 2007; Wen et al., 2011; Yaswen and Campisi, 2007) and as a novel metastasis suppressor by preventing early dissemination *via* the maintenance of E-cadherin junctions and inhibition of an EMT-like program. This is different from the dormancy-inducing function we reported for p38α/β in aggressive HNSCC DTCs that enter a microenvironment-driven dormancy in the bone marrow (Bragado et al., 2013; Sosa et al., 2015). How HER2 and Wnt crosstalk to inhibit p38 is not clear, but HER2 inhibition restored P-ATF2 and E-cadherin levels. However, whether this is WNT-dependent is unclear. One possibility is that HER2, PgR and/or Wnt signaling regulate the expression of p38 phosphatases such as Wip1 or DUSP-1 (Bulavin et al., 2002).

Early stage lesions in adult mice were presumed to be mainly sessile and thus, imaging cell motility during these stages was never attempted. Imaging small areas of the ductal tree showed that during the pre-malignant stage (week 15-18) individual HER2-CFP early cancer cells were found

detaching from the ductal tissue and translocating in multiple directions in what resembled an amoeboid-like movement (Bailly et al., 1998; Friedl and Brocker, 2000; Hall et al., 1989). All these events of invasion were clearly originating from the ductal structures, because while MMTV-Cre-mediated recombination can occur outside of mammary tissues (Wagner et al., 2001) we could not detect any CFP cells randomly passing through the imaging fields within the stroma of all control and SB203580 treated mice. This invasive capacity of early cancer cells was further observed when it was vigorously stimulated by systemic p38α/β inhibition. HER2-CFP early cancer cells showed active cell projections and translocated outside the epithelial layers but also inside ducts. Interestingly, local invasion was never observed to be collective as observed in 3D systems, including ours ((Cheung et al., 2013) and **Fig3**). Invadopodia formation local invasion and intravasation have been elegantly documented in invasive mammary tumors (Dovas et al., 2011; Lorenz et al., 2004; Oser et al., 2009). Our intra-vital imaging now shows that these events are not an exclusive property of advanced tumor cells from overt lesions and that HER2 signaling controls the invasive behavior in a subpopulation of early cancer cells despite having less evolved genomes (Hosseini et al,). It is unknown whether the EMT program of early DCCs is the same as in advanced cancer cells but it is possible that eDCCs tap into amoeboid mechanisms or motility activated in confined epithelial cells (Liu et al., 2015).

Our work supports the hypothesis that during long periods of the natural history of mammary cancer, and most unexpectedly during early stages, there are distinct mechanisms which drive the dissemination of a specific subpopulation of early cancer cells. This suggests the existence of a large heterogeneity of DCCs from arising from all stages of progression, including vast numbers of non-cycling eDCCs. Further analysis is required to determine whether these cells display dormancy characteristics (Sosa et al., 2014). A difficult question to answer is whether early progressed lesions contribute to metastasis and how to detect this contribution? One possibility is that the identified mechanisms are recapitulated in certain patients as shown by Hosseini et al,. The other may come from detailed analysis of a well genetically annotated case study by Haffner et al., (Haffner et al., 2013). The authors reported that in a prostate cancer patient, 7 metastases resected 17 years after

radical prostatectomy showed evolutionary traits that could be traced back to a small low-grade subpopulation of cells in the primary tumor, not from the rest of the tumor deemed more “aggressive” by pathology. Thus, early invasive cells in the primary site could disseminate early and eventually form metastases that did not evolve in the same way as the rest of the primary tumor clones. Such analysis could be performed in breast cancer lesions.

Overall, our work identifies a new mechanism by which interplay between HER2 and p38 signaling regulates not only tumor onset but also metastatic progression by regulating the capacity of early progressed cancer cells to disseminate to target organs. This suggests that tumor suppressor pathways such as p38, might have previously unrecognized metastasis suppressive function by blocking early dissemination. Metastasis suppressor signals, including the p38 pathway(Taylor et al., 2008), had been mostly attributed to genes that would affect metastatic onset but not primary tumor growth(Shoushtari et al., 2011). Our work changes the scale of the timing of metastasis suppressor pathway function and the origin of metastasis. These may have important implications in the treatment of lethal breast cancer metastasis as systemic adjuvant therapies targeting the DCCs and overt metastasis might need to take into account this heterogeneity.

EXPERIMENTAL PROCEDURES.

See **Supplemental Experimental Procedures** for additional procedures

Cells and cell culture. MCF10A-HER2 cells expressing sFRP were generated using sFRP lentiviral vectors. Wnt3a and DKK1 conditioned media was prepared from Wnt3a expressing L-cells and Dkk1 expressing 293T cells. Vectors and sFRP plasmids were a kind gift from Dr. Stuart Aaronson, ISMMS, New York, NY. Conditioned media was prepared from cells cultured with serum free medium (DMEM + 1%P/S) for 24 hours and then concentrated using Vivaspin 20 Centrifugal Concentrating tubes (Sartorius, VS2021) at 3000g up to 3 hours until desired concentration (10x) was reached.

Mammospheres and tumorspheres assays. Animal procedures were approved by the Institutional Animal Care and Use Committee (IACUC) of Icahn School of Medicine at Mount Sinai protocol 08-0366. MMTV-HER2 mice were sacrificed using CO_2 at age 14-18wk or when overt tumors had formed (PT). For mammosphere preparations, all 5 pairs of glands in mice were checked for the presence of any visible small lesions or palpable tumors when processed for early cancer cell and none were found. Even when other mammary glands were inspected microscopically in whole mounts we could not detect small tumors. Whole mammary glands or tumors were digested in Collagenase/BSA at 37°C for 45-60min. Red blood cell lysis buffer was used to remove blood cells from cultures and cells were then plated for 10-15min in DMEM+10%FBS in 35mm dishes at 37°C to for fibroblast removal. Cells were then incubated in PBS-EDTA 2mM for 15min at 37°C and passed through a 25 gauge needle. Cell suspensions were then filtered through a 70μM filter before counting. Cells were seeded in 6-well ultra low adhesion plates at a density >$5.0x10^5$ cells per well in 1mL mammosphere media (DMEM/F12 (Gibco 11320-082), 1:50 B27 (Invitrogen 17504-044), EGF (Peprotech AF-100-15-A), 1:100 Pen/Strep). Approximately 300 spheres were injected per site. Suspension cultures were spun at 300rpm for 4min and then suspended in 150ul PBS++/300 spheres. Matrigel (Corning 356231) was then added in a 1:1 ratio. Spheres were injected into the two 4^{th} inguinal gland fat pad using a 27-gauge needle.

3D mammary primary epithelial cell cultures. MMTV-HER2 mice were sacrificed using CO_2 at age 14-18wk and MECs were isolated using the same protocol used for mammosphere preparation.). Similar to mammosphere preparations, all 5 pairs of glands in mice were checked for the presence of any visible or palpable tumors when processed for early cancer cell and none were found even in whole mounts prepared from mammary glands from the same mouse processed for mammoprsphere preparation. 5.0X10^4 MECs were seeded in in 400ul Assay Medium in 8-well chamber slides with 40ul of Matrigel. Acini formed at an efficiency of around 30 acini/$1.0x10^4$ MECs plated. Cultures were treated every 24 hours with 5uM DMSO/SB203580 and 500ng/ml DKK1 for 48 hours following acini

formation and fixed for immunofluorescence (IF) with 4%PFA or 10% Formalin with phosphatase and protease inhibitors.

Patient samples. Paraffin embedded sections from DCIS and invasive breast cancer patient tumors were obtained from the Cancer Biorepository at Icahn School of Medicine at Mount Sinai, New York, NY. Samples were de-identified and obtained with Institutional Review Board approval, which indicated that this work does not meet the definition of human subject research according to the 45 CFR 46 and the Office of Human Subject Research. IF and immunohistochemistry (IHC) analysis was done using samples from 10 DCIS and 20 invasive breast cancer patients. Invasive breast cancer samples included Luminal A, B and HER2 positive subtypes.

Circulating Cancer Cells (CCCs) and Disseminated Cancer Cells (DCCs) detection. 16 week-old MMTV-HER2 mice were treated with SB (10 mg/kg) or DMSO for 2 weeks and blood was drawn by cardiac puncture following IACUC protocols. CCCs were purified using negative lineage cell-depletion kit (Cat 130-090-858, Milteny) fixed and stained with anti-CK8/18 antibody in cytospin preparations. Bone marrow cells from 4 long bones were flushed out Minimum Essential Medium Eagle (MEME) (Sigma, MO, USA) using 26-G needle and 1 ml syringe. Tumor cells were enriched by Ficoll-Paque plus (GE Healthcare) density gradient separation and filtered through 30uM nylon mesh to remove large aggregates. Cells were fixed with 3% PFA for 20 min on ice and cytospin preparations were carried out by centrifugation of bone marrow cells at 500 rpm for 3 min using poly-L-lysine-coated slides (Sigma, MO, USA). DCCs were stained with anti-CK8/18 or anti-HER2 antibodies in cytospin preparations were analyzed. We screened 0.5-2.0x10^6 BM cells, which represents 20% of the total BM cells per mouse and then normalized to 1x10^6 BM cells. Similar to mammosphere preparations, all 5 pairs of glands in mice were checked for the presence of any visible or palpable tumors when processed for early cancer cell and none were found as described above.

Intra-vital microscopy. Imaging of 3D acini was done using confocal microscopy. Images were obtained using Leica Software on a Leica SP5 confocal microscope. Mammary gland section imaging was done using Leica DM 550 fluorescence microscope using Leica Software. Dye Separation analysis was done using Leica Software. 2-photon imaging was performed following the reported protocols (Entenberg et al., 2011). Intravital imaging was performed using a custom-built two-laser multiphoton microscope following previously reported imaging protocols(Entenberg et al., 2011). All procedures were conducted in accordance with the National Institutes of Health regulations and approved by the Albert Einstein College of Medicine animal use committee. More detailed description of two-photon imaging can be found in Supplemental Experimental Procedures.

Statistical Analysis. Statistical Analysis was done using Prism Software. Differences were considered significant if *P* values was <0.05. For all cell cultures, one tailed *student t-tests* were performed. For mouse experiments one tailed *Mann-Whitney* tests were used.

AUTHORS CONTRIBUTIONS. KH: designed, optimized and performed experiments, analyzed data and co-wrote the manuscript, MSS: designed and optimized experimental approach, performed experiments, designed and executed intravital imaging experiments, provided guidance and oversight, analyzed data and co-wrote the manuscript, HH: designed and performed experiments and analyzed data, AAV: performed experiments, CN: provided human histological samples and provided histopathological analysis, RD: provided mouse mammary gland samples, CK: designed experiments, analyzed data and co-wrote the manuscript, DE: designed and executed intravital imaging, analyzed data and co-wrote the manuscript. JC: designed intra-vital experiments, analyzed data and co-wrote the manuscript, EFF: provided expertise in the MMTV-HER2 model, deigned experiments and analyzed data, JAA-G: designed and optimized experimental approach, provided general guidance and oversight, analyzed data and co-wrote the manuscript.

Acknowledgements. We thank the Aguirre-Ghiso, Klein and Condeelis labs for useful discussions. Grant Support: Samuel Waxman Cancer Research Foundation Tumor Dormancy Program to J.A.A-G. and E.F.F., NIH/NCI (CA109182) to J.A.A-G., NCI - Tumor Microenvironment Network (CA163131) to J.A.A-G and J.C., NIH/NCI F31 CA183185 to K.H., DoD-BCRP Breakthrough Award (BC132674) to J.A.A-G and J.C., DoD-BCRP Grant (BC112380) to M.S.S.

REFERENCES:

Bailly, M., Yan, L., Whitesides, G.M., Condeelis, J.S., and Segall, J.E. (1998). Regulation of protrusion shape and adhesion to the substratum during chemotactic responses of mammalian carcinoma cells. Experimental cell research *241*, 285-299.

Bhoumik, A., Fichtman, B., Derossi, C., Breitwieser, W., Kluger, H.M., Davis, S., Subtil, A., Meltzer, P., Krajewski, S., Jones, N.*, et al.* (2008). Suppressor role of activating transcription factor 2 (ATF2) in skin cancer. Proc Natl Acad Sci U S A *105*, 1674-1679.

Brabletz, T. (2012). To differentiate or not--routes towards metastasis. Nature reviews Cancer *12*, 425-436.

Bragado, P., Estrada, Y., Parikh, F., Krause, S., Capobianco, C., Farina, H.G., Schewe, D.M., and Aguirre-Ghiso, J.A. (2013). TGF-beta2 dictates disseminated tumour cell fate in target organs through TGF-beta-RIII and p38alpha/beta signalling. Nat Cell Biol *15*, 1351-1361.

Brisken, C., Heineman, A., Chavarria, T., Elenbaas, B., Tan, J., Dey, S.K., McMahon, J.A., McMahon, A.P., and Weinberg, R.A. (2000). Essential function of Wnt-4 in mammary gland development downstream of progesterone signaling. Genes Dev *14*, 650-654.

Bulavin, D.V., Demidov, O.N., Saito, S., Kauraniemi, P., Phillips, C., Amundson, S.A., Ambrosino, C., Sauter, G., Nebreda, A.R., Anderson, C.W.*, et al.* (2002). Amplification of PPM1D in human tumors abrogates p53 tumor-suppressor activity. Nature genetics *31*, 210-215.

Bulavin, D.V., and Fornace, A.J., Jr. (2004a). p38 MAP kinase's emerging role as a tumor suppressor. Advances in cancer research *92*, 95-118.

Bulavin, D.V., Phillips, C., Nannenga, B., Timofeev, O., Donehower, L.A., Anderson, C.W., Appella, E., and Fornace, A.J., Jr. (2004b). Inactivation of the Wip1 phosphatase inhibits mammary tumorigenesis through p38 MAPK-mediated activation of the p16(Ink4a)-p19(Arf) pathway. Nature genetics *36*, 343-350.

Cheung, K.J., Gabrielson, E., Werb, Z., and Ewald, A.J. (2013). Collective invasion in breast cancer requires a conserved basal epithelial program. Cell *155*, 1639-1651.

Debnath, J., Mills, K.R., Collins, N.L., Reginato, M.J., Muthuswamy, S.K., and Brugge, J.S. (2002). The role of apoptosis in creating and maintaining luminal space within normal and oncogene-expressing mammary acini. Cell *111*, 29-40.

Dovas, A., Gligorijevic, B., Chen, X., Entenberg, D., Condeelis, J., and Cox, D. (2011). Visualization of actin polymerization in invasive structures of macrophages and carcinoma cells using photoconvertible beta-actin-Dendra2 fusion proteins. PloS one *6*, e16485.

Entenberg, D., Wyckoff, J., Gligorijevic, B., Roussos, E.T., Verkhusha, V.V., Pollard, J.W., and Condeelis, J. (2011). Setup and use of a two-laser multiphoton microscope for multichannel intravital fluorescence imaging. Nature protocols *6*, 1500-1520.

Friedl, P., and Brocker, E.B. (2000). The biology of cell locomotion within three-dimensional extracellular matrix. Cellular and molecular life sciences : CMLS *57*, 41-64.

Grumolato, L., Liu, G., Mong, P., Mudbhary, R., Biswas, R., Arroyave, R., Vijayakumar, S., Economides, A.N., and Aaronson, S.A. (2010). Canonical and noncanonical Wnts use a common mechanism to activate completely unrelated coreceptors. Genes Dev *24*, 2517-2530.

Haffner, M.C., Mosbruger, T., Esopi, D.M., Fedor, H., Heaphy, C.M., Walker, D.A., Adejola, N., Gurel, M., Hicks, J., Meeker, A.K.*, et al.* (2013). Tracking the clonal origin of lethal prostate cancer. The Journal of clinical investigation *123*, 4918-4922.

Hall, A.L., Warren, V., Dharmawardhane, S., and Condeelis, J. (1989). Identification of actin nucleation activity and polymerization inhibitor in ameboid cells: their regulation by chemotactic stimulation. The Journal of cell biology *109*, 2207-2213.

Husemann, Y., Geigl, J.B., Schubert, F., Musiani, P., Meyer, M., Burghart, E., Forni, G., Eils, R., Fehm, T., Riethmuller, G.*, et al.* (2008). Systemic spread is an early step in breast cancer. Cancer Cell *13*, 58-68.

Klein, C.A. (2010). Framework models of tumor dormancy from patient-derived observations. Current opinion in genetics & development.

Klemke, R.L., Cai, S., Giannini, A.L., Gallagher, P.J., de Lanerolle, P., and Cheresh, D.A. (1997). Regulation of cell motility by mitogen-activated protein kinase. The Journal of cell biology *137*, 481-492.

Liu, Y.J., Le Berre, M., Lautenschlaeger, F., Maiuri, P., Callan-Jones, A., Heuze, M., Takaki, T., Voituriez, R., and Piel, M. (2015). Confinement and low adhesion induce fast amoeboid migration of slow mesenchymal cells. Cell *160*, 659-672.

Lorenz, M., Yamaguchi, H., Wang, Y., Singer, R.H., and Condeelis, J. (2004). Imaging sites of N-wasp activity in lamellipodia and invadopodia of carcinoma cells. Current biology : CB *14*, 697-703.

Maekawa, T., Shinagawa, T., Sano, Y., Sakuma, T., Nomura, S., Nagasaki, K., Miki, Y., Saito-Ohara, F., Inazawa, J., Kohno, T.*, et al.* (2007). Reduced levels of ATF-2 predispose mice to mammary tumors. Molecular and cellular biology *27*, 1730-1744.

Nelson, C.M., Vanduijn, M.M., Inman, J.L., Fletcher, D.A., and Bissell, M.J. (2006). Tissue geometry determines sites of mammary branching morphogenesis in organotypic cultures. Science *314*, 298-300.

Oser, M., Yamaguchi, H., Mader, C.C., Bravo-Cordero, J.J., Arias, M., Chen, X., Desmarais, V., van Rheenen, J., Koleske, A.J., and Condeelis, J. (2009). Cortactin regulates cofilin and N-WASp activities to control the stages of invadopodium assembly and maturation. The Journal of cell biology *186*, 571-587.

Pearson, G.W., and Hunter, T. (2007). Real-time imaging reveals that noninvasive mammary epithelial acini can contain motile cells. The Journal of cell biology *179*, 1555-1567.

Schardt, J.A., Meyer, M., Hartmann, C.H., Schubert, F., Schmidt-Kittler, O., Fuhrmann, C., Polzer, B., Petronio, M., Eils, R., and Klein, C.A. (2005). Genomic analysis of single cytokeratin-positive cells from bone marrow reveals early mutational events in breast cancer. Cancer Cell *8*, 227-239.

Shamir, E.R., Pappalardo, E., Jorgens, D.M., Coutinho, K., Tsai, W.T., Aziz, K., Auer, M., Tran, P.T., Bader, J.S., and Ewald, A.J. (2014). Twist1-induced dissemination preserves epithelial identity and requires E-cadherin. The Journal of cell biology *204*, 839-856.

Shoushtari, A.N., Szmulewitz, R.Z., and Rinker-Schaeffer, C.W. (2011). Metastasis-suppressor genes in clinical practice: lost in translation? Nature reviews Clinical oncology *8*, 333-342.

Sosa, M.S., Bragado, P., and Aguirre-Ghiso, J.A. (2014). Mechanisms of disseminated cancer cell dormancy: an awakening field. Nature reviews Cancer *14*, 611-622.

Sosa, M.S., Parikh, F., Maia, A.G., Estrada, Y., Bosch, A., Bragado, P., Ekpin, E., George, A., Zheng, Y., Lam, H.M.*, et al.* (2015). NR2F1 controls tumour cell dormancy via SOX9- and RARbeta-driven quiescence programmes. Nat Commun *6*, 6170.

Su, G.H., Song, J.J., Repasky, E.A., Schutte, M., and Kern, S.E. (2002). Mutation rate of MAP2K4/MKK4 in breast carcinoma. Human mutation *19*, 81.

Taylor, J.L., Szmulewitz, R.Z., Lotan, T., Hickson, J., Griend, D.V., Yamada, S.D., Macleod, K., and Rinker-Schaeffer, C.W. (2008). New paradigms for the function of JNKK1/MKK4 in controlling growth of disseminated cancer cells. Cancer letters *272*, 12-22.

Teng, D.H., Perry, W.L., 3rd, Hogan, J.K., Baumgard, M., Bell, R., Berry, S., Davis, T., Frank, D., Frye, C., Hattier, T.*, et al.* (1997). Human mitogen-activated protein kinase kinase 4 as a candidate tumor suppressor. Cancer Res *57*, 4177-4182.

Thiery, J.P., Acloque, H., Huang, R.Y., and Nieto, M.A. (2009). Epithelial-mesenchymal transitions in development and disease. Cell *139*, 871-890.

Ventura, J.J., Tenbaum, S., Perdiguero, E., Huth, M., Guerra, C., Barbacid, M., Pasparakis, M., and Nebreda, A.R. (2007). p38alpha MAP kinase is essential in lung stem and progenitor cell proliferation and differentiation. Nature genetics *39*, 750-758.

Wagner, K.U., McAllister, K., Ward, T., Davis, B., Wiseman, R., and Hennighausen, L. (2001). Spatial and temporal expression of the Cre gene under the control of the MMTV-LTR in different lines of transgenic mice. Transgenic research *10*, 545-553.

Wen, H.C., Avivar-Valderas, A., Sosa, M.S., Girnius, N., Farias, E.F., Davis, R.J., and Aguirre-Ghiso, J.A. (2011). p38alpha Signaling Induces Anoikis and Lumen Formation During Mammary Morphogenesis. Science signaling *4*, ra34.

Yaswen, P., and Campisi, J. (2007). Oncogene-induced senescence pathways weave an intricate tapestry. Cell *128*, 233-234.

FIGURE LEGENDS:

Figure 1: HER2+ cancer cells disseminate early and form metastasis. (A) Circulating cancer cells (CCCs) were isolated from blood of HER2 mice at early stages of cancer progression (age 14-18wk) and cytospin preparations were stained for the epithelial marker CK8/18 (green) and nuclei with DAPI (blue). # CTCs/mL blood in mice can be found in **S-Fig 1**. Scale bar=10μM **(B)** IHC for HER2 on lung sections from MMTV-HER2 mice (age 14-18wk) was used to detect early disseminated cancer cells (DCC) within the lung (scale bar=25μM). Regions (i and ii) are augmented in the panel images (right). Empty arrowheads indicate HER2+ DTCs and filled arrowheads point to host HER2- cells within the lung (scale bar=10μM). Number of HER2+ DTCs/field can be found in **S-Fig1**. **(C)** Disseminated cancer cells (DCCs) in the bone marrow of MMTV-HER2 mice were extracted from four hind limb long bones (age 14-18wk). DCCs were detected in cytospin preparations of whole bone marrow samples by staining for the epithelial marker CK8/18 (green), HER2 (red) and nuclei with DAPI (blue).

Cells, which were CK8/18+, HER2+ or +/+ were considered eDCCs. The total # of eDCCs/bone marrow can be found in **S-Fig1**. Right panels show individual channel signals and the merged channels are shown on the left detecting a BM CK8/18+/HER2+ DTC (empty arrowhead) next to a CK8/18-/HER2- bone marrow cell (full arrowhead). Scale bar=10μM. **(D)** IF using antibodies for HER2 (red/yellow) to detect DTCs, p-Rb (green) as a marker of proliferation, and DAPI (blue) for nuclei in lung sections from MMTV-HER2 mice at early stages of progression (age 14-18wks) and mice with overt tumors (age 25wk and up). Early DCCs (eDCC) were detected in 14-18wk MMTV-HER2 mice (middle and right top panels). IgG control for HER2 in **S-Fig 1**. Lungs carrying a mixture of early and late (e/L) DCCs found in mice bearing overt tumors (bottom middle and right panels). *Lower two panels*, Tumor (right) and metastases (left) sections stained for HER2 (red) and p-Rb (green). Scale bars=10μM. **(E)** Table showing the tumorigenic and metastatic efficiency of sphere cultures prepared from MMTV-HER2 mice and injected into nude mice as outlined in **S-Fig 1**. Primary tumor incidence (PT) as well as lung macro-metastases (Mets) in these mice was monitored up to one year. Tumorsphere injected mice were sacrificed by 3 months due to large tumor size with no detectable lung macro-metastases. Mammosphere injected mice were tracked up to a year with no primary tumor incidence while 3/14 mice had detectable lung macro-metastases. **(F)** H&E staining for sections of lung metastasis found in nude mice injected with MMTV-HER2 mammospheres (*upper left*). *Upper right*, shows differentiated glandular ductal structures found within the same metastasis. *Bottom panel*, representative image of P-Rb levels (green) and HER2 (red) staining in a micro-metastasis from mammosphere injection. Scale bar=10μM (top right, bottom image), 100 μM (top left image). **(G)** The % of P-Rb positive HER2-DTCs was quantified in mice with early lesions (E) overt tumors (E/L) (n>200cells). Single DTCs were considered when $\leq$3 HER2+ DTCs were found solitary or a cluster (2-3 HER2+cells). The % of p-Rb cells within metastases was also quantified in HER2 mice carrying over tumors as shown in **Fig 1D** (Met) (n=5 metastasis) or in metastases initiated from injection of MMTV-HER2 mammospheres as seen in **Fig 1F** (n=11 micro, n=4 macro). Micro-

metastases were considered as clusters ranging from 3-20 cells. Macro-metastases were clusters >20 cells. Values = mean % p-Rb + cells with error bars representing ± SEM. *=p<0.05

Figure 2: E-cadherin, HER2 and p38 activation in early and invasive breast cancer cells. (A) Early stage MMTV-HER2 mammary gland sections (age 14-18wk) co-stained for E-cadherin (green) and p-ATF2 (red). Representative images of E-cad^{hi}/p-ATF2^{hi} (TOP) and E-cad^{LOW}/p-ATF2^{LOW} (BOTTOM) ducts in MMTV-HER2 mammary ducts are shown (scale bar=25μM). Middle four panels, heterogeneity for E-cad and P-ATF2 signals: P-ATF2^{HIGH}/E-cad^{HIGH} cells (left column) and p-ATF2^{LOW}/E-cad^{LOW} cells (right column) in the MMTV-HER2 and MMTV-HER2-T (Balb-Neu-T, 15 weeks old) models (scale bar=10μM). Empty arrows highlight examples of P-ATF2^{HIGH}/E-cad^{HIGH} cells within a duct. Full arrows point to p-ATF2^{LOW}/E-cad^{LOW} cells (scale bars=10 μM). *Left graph*, the heterogeneity for P-ATF2 and E-cadherin signals was quantified by determining the percent of E-cad^{HI} cells/duct that were P-ATF2$^{HI/LO}$. Values represent mean with errors bars representing SEM. (HER2 n=30 ducts; HER2-T n=10 ducts). (B) Top and bottom panels, early stage MMTV-HER2 mammary glands co-stained for E-cadherin (green), HER2 (red) and DAPI (blue). Empty arrows indicate HER2^{HIGH}/E-cad^{LOW} cells and full arrows indicate HER2^{LOW}/E-cad^{HIGH} cells. Bottom panel further illustrates the inter-ductal heterogeneity of E-cadherin and HER2. Inset in bottom panel shows detailed image of boxed region. (Scale bar=10 μM inset, 25 μM panels). Graph shows the percentage of HER2^{HIGH} cells that were E-cadherin$^{LOW/HIGH}$ (n=20 ducts, 2 mice). (C) Representative images of DCIS patient samples parallel sections stained for p-ATF2 (Red) HER2 (Green – insets lower row), E-cadherin (green – also insets upper row). Patients were categorized as HER2 positive or negative by IF for HER2 (insets lower row, green). Inset images show detail of E-cadherin junctions in HER2+ and HER2- patients with the empty arrows indicating strong E-cadherin junctions and a full arrow highlighting weak E-cadherin staining. (Scale bars=25μM, 10 μM for inset). Metamorph software was used to quantify HER2, E-cadherin and p-ATF2 fluorescence signal intensity in DCIS samples. Mean fluorescence intensity (m.f.i)/cell/field in HER2+ (black bars) vs. HER2- (grey bars) patients is represented in the graph (right) with error bars representing SEM values. (n=10 patients) (D) Western

blot for the indicated antigens in lysates of FvB MECs isolated from normal mammary glands and tumor cells isolated from MMTV-HER2 overt primary tumors. GAPDH was used as an additional loading control. (E) Quantification of IHC for P-p38 and P-ATF2 performed on invasive breast cancer patient samples (images found in **S-Fig2**). Patients were classified as HER2+/- as provided by the pathologist. Metamorph software was used to determine the mean fluorescence intensity (m.f.i) per field for P-p38 and P-ATF2. P-p38 intensity in HER2+/- patients is shown on the left axis and first two columns of the graph. p-ATF2 intensity is shown in the right hand axis and last two columns on the graph. Error bars represent SEM, n=5 patients/group. (F) MCF10A-HER2 MECs were treated in culture with 100nM Lapatinib or DMSO for 24 hours. Representative images are shown of IF staining for P-ATF2 (Red) and E-cadherin (Green) (Scale bars= 10μM). Quantification of the percent (%) of P-ATF2 positive cells in Lapatinib treated cultures compared to DMSO controls is shown in the graph (right). Boxplot showing median and range (n=300 cells/treatment, 3 biological replicates) *=p<0.05 , **=p<0.01, ***=p<0.0001.

Figure 3: HER2^{+} early cancer cells are E-cadherin^{LOW} and micro-invasive. (A) MCF10A-HER2 cells cultured in 3D Matrigel were stained for E-cadherin (green) and DAPI (blue). A representative image of acini, left panel (Scale bar=25 μM). Details of E-cad^{lo} cells microinvading are shown to the right (top and bottom). Empty arrows indicate E-cad^{lo} cells invading outward from colonies (Scale bar=10 μM). Around 40% of MCF10A-HER2 acini show outward invasion of one cell/colony in equatorial sections (**Fig 3D**). 92$\pm$8.3% of outward invading cells were E-cadherin^{LOW} (n= 20 acini). **(B)** Ealry MMTV-HER2 mammary gland sections (age 14-18wk) co-stained for E-cadherin (green), HER2 (red) and DAPI (blue). Empty arrows indicate HER2^{+}/E-cad^{LOW} cells invading into stroma or out from epithelial layers in ducts. The percent (%) of outward invading cells, which were E-cad^{LOW} is shown. (n=54-63 cells/mammary gland section, 2 mice) **(C)** MMTV-HER2 MECs were isolated from the mammary glands of 14-18 weeks-old mice before mice had developed tumors. Following formation of acinar-like structures cultures were treated for 48hr with DMSO or 5μM of the p38α/β inhibitor SB203580. Zoomed regions on the right show the presence of invasive cells only found in SB203580-

treated cultures. MMTV-HER2 3D cultures were stained for F-actin (red), Laminin V (green) and DAPI (blue). Empty arrows highlight invasive events; a full arrow indicates intact laminin-V layer in DMSO controls. Quantification of the number of acini with outward invasion in DMSO (C) and SB203580 treated cultures is shown in the graph to the right (DMSO=11; SB=9). Scale bars=25μM **(D)** MCF10A-HER2 cells were seeded in 3D Matrigel and treated for 6 days with the p38 inhibitor SB203580 following acini formation (day 4). Representative images of acini stained for f-actin (red) and Laminin-V (green). Quantification of the percent (%) of acini with outward invasion is shown with error bars representing the SEM. (n=109 acini DMSO, 87 acini SB203580) ***=p<0.001

Figure 4: p38 inhibition promotes EMT markers in HER2+ early cancer cells. (A) MCF10A-HER2 and early MMTV-HER2 MECs were cultured in 3D Matrigel and treated for 6 days and 48 hrs, respectively with the p38α/β inhibitor SB203580 following acini formation. Acini were stained for E-cadherin and β-catenin. Gray scale images in the right MMTV-HER2 panel show magnification of MMTV-HER2 acini for a more detailed view of membrane localized β-catenin. Top right graph panel, shows the quantification of E-cad^{HIGH} and β-cat^{MEM} acini: % E-cadherin is on the left axis (green bars) and %β-catenin in the membrane is on the right axis (red bars). (MCF10A-HER2 n=20acini/treatment, MMTV-HER2 n=10 acini/treatment) scale bars=25μM **(B)** Effect of genetic inhibition of p38α signaling on E-cadherin and β-catenin-based junctions. MCF10A-HER2 (*Left panels*) and MMTV-HER2 cells (*Middle panels)* were cultured in 3D Matrigel and treated as in **A** but with siRNAs targeting p38α as well as a non-targeting control (siCTL). Results were similar to what was seen with the pharmacological inhibitor, SB203580. Quantification of E-cad^{HIGH} and β-cat^{MEM} is shown in the right bottom graph panel in **A** (MCF10A-HER2 n=20 acini/treatment, MMTV-HER2 E-cadherin=30 acini/treatment, □-catenin=10 acini/treatment). Acini were also stained in one trial with an antibody recognizing the active conformation of β-catenin (see methods). Quantification of acini, which were strongly stained with this antibody, is shown in the top right panel (n=10 acini/treatment). scale bars=25μM **(C)** AXIN2 mRNA levels were measured in MCF10A-HER2 monolayer cultures treated for 24 hours with DMSO control (C) or SB203580 (SB, 5μM). Samples were run in triplicate and values

were normalized to GAPDH and fold change over control was determined for five biological replicates. **(D)** Early stage MMTV-HER2 (age 14-18 week) and MMTV-HER2-T (Balb-NeuT age 15 week) mammary gland sections stained for HER2 and β-catenin. Left and right panels show two separate duct examples. Full arrows indicate $HER2^{+}$/β-$catenin^{MEM\text{-}LOW}$ MECs found within the duct while empty arrows highlight $HER2^{-}$/β-$catenin^{MEM\text{-}HIGH}$ MECs (Scale bars=25 μM). The percent (%) of β-$catenin^{MEM\text{-}HIGH}$ and $HER2^{+/-}$ cells per duct was quantified in HER2 and HER2-T and shown in **S-Fig4**. Digital dye separation Leica software module was used on the images. **(E)** Lung sections from MMTV-HER2 mice (age16-20 wks) carrying only early DCCs were stained for HER2 (red), E-cadherin (green) and DAPI (blue) to detect E-cadherin levels in HER2+ DTCs. 98 $\pm$ 0.57% of HER2+ DTCs were E-cadherin negative ($n \geq 100$ DTCs, 3 mice). Scale bar=10 μM, *=$p<0.05$

Figure 5: Effect of p38 inhibition on EMT markers and early dissemination of HER2+ cancer cells *in vivo*. (A-B) Mammary glands from early stage MMTV-HER2 mice treated for 2 weeks with the p38α/β inhibitor SB203580 (age 16-18 weeks, 10mg/kg, i.p every 48hr) were stained for E-cadherin (**A**) and β-catenin (**B**). Boxed areas are magnified in the lower row (Scale bars=10 μM). Empty arrows indicate strong membrane localized β-catenin and full arrows indicate nuclear events in SB203580 mice (Scale bar=10 μM). Quantification of the average % of $E\text{-}cad^{HIGH}$ ducts in DMSO (C) and SB203580 treated mice and % of nuclear events/duct is shown in the bottom graph (n=4 mice). **(C)** Whole blood was extracted post-euthanasia from MMTV-HER2 mice (age 14-18wk) treated for two weeks with DMSO (C) or the p38α/β inhibitor SB203580. CCCs were detected as CK8/18+ as in **Fig 1A** and plotted in the graph. Following SB203580 treatment the number of CCCs significantly increased in MMTV-HER2 mice (n=5 mice). **(D)** Bone marrow samples were collected from two tibias and two femurs of mice treated with DMSO (C) or the p38α/β inhibitor SB203580 as in **A**. Early DCCs that were CK8/18+ and HER2+ or co-stained for both markers in cytospin preparations were quantified and the # of DTC in whole bone marrow is shown in the graph. SB203580 treatment resulted in a significant increase of bone marrow eDCCs (n=5mice/group). The median # of eDCCs in this BM compartment is comparable to ~1.3 eDCCs/ 10^6 BM host cells in control groups and ~8

eDCCs/10^6 BM host cells in SB203580 treated animals. **(E)** DCCs were detected in the lung of early MMTV-HER2 mice treated with DMSO (C) or the p38α/β inhibitor SB203580 as in **Fig 1B**. The number of HER2+ DCCs/field is shown for both DMSO (C) and SB203580 treated mice (n=30 fields, 3 mice/treatment). *p<0.05, **=p<0.01

Figure 6: High resolution 2-photon intra-vital imaging of early dissemination. (A) Stills from intra-vital movies of 10 (left, S-Movie 1), 15 (middle, S-Movie 2) and 18 (right, S-Movie 3) weeks old mammary glands of MMTV-HER2-CFP mice. Blue-white signal pinpoints the CFP+ cells while rhodamine-dextran injected i.v. highlights the vasculature. No events of micro-invasion were observed at 10 wks, while at 15 and 18 weeks micro-invasion and motility were evident. Inset in the left panel shows a detail of a CFP+ duct. The arrows and outlines in the middle 15 wks panel shows CFP+ cells actively microinvading and translocating. Sequence inset in the right 18 wks panel shows active microinvasion and travel of a early cancer cells. Dotted arrow= director of movement. **(B)** Stills from intra-vital movies of a duct from an MMTV-HER2-CFP mice treated with SB203580 for 2 weeks as in Fig5A (S-Movie 4). Note the disorganized ductal structure compared to A and in the inset CFP+ early cancer cells displaying invadopodia like projections towards the blood vessel. The full arrow in B points to a blood vessel where an intravasation event was filmed and a sequence is shown in the images that span below B and C (S-Movie 5). Dotted line direction of movement and full arrow point out the CFP+ intravasating cell. **(C)** Low power intra-vital still from movie of a early stage duct of MMTV-HER2-CFP mice treated with SB203580 for 4 weeks where events of micro-invasion (full arrows and S-Movie 6) and intravasation are observed (S-Movie 6 and 7). **(D)** *Top panel, h*igh power high resolution intra-vital still from a movie of the area boxed in C showing active breaching of MMTV-HER2-CFP cells from the ductal structure into the stroma and interacting with blood vessels (red) (S-Movie 8). *Middle and bottom panels*, frames of a 3D computer generated reconstruction of the movie in D, top panel (S-Movie 8). The middle panel shows the same projection and the bottom panel a rotated projection to show the interaction (yellow) between early cancer cells (CFP) and blood vessels (red) (S-Movie 9).

Figure 7: HER2 and p38 regulate a Wnt-driven EMT-like program in early cancer cells. (A) MCF10A and MCF10A-HER2 cells were plated in 3D Matrigel and treated from day 6-12 with the p38α/β inhibitor SB203580 (5μM). Gene expression profiling for 86 EMT target genes was performed as described in Experimental Procedures. A 14-gene EMT signature (right gene list) was generated from genes upregulated > 2 fold over three trials and plotted using Gene-E. Green columns represent control values set to 1 and fold change over control is shown in red for each gene. **(B)** Q-PCR array measurement of *E-Cadherin* mRNA levels in MCF10A-HER2 acini treated for 6 days with SB203580 (5μM) and sip38α (20nM). Samples were run in triplicate and normalized to GAPDH. Fold change over control is shown. DMSO was used as a control for SB203580 samples and, non-targeting siRNA was used as a control for sip38α. *Twist* mRNA levels were measured in RNA extracted from early MMTV-HER2 mammary glands (age 14-18wk) treated for 2 weeks with vehicle or SB203580 (10mg/kg, i.p every 48hr). Fold change over control (DMSO) is shown with values normalized to GAPDH (n=3 mice/treatment); left Y-axis for E-cadherin and right Y-axis for Twist. **(C)** MCF10A-HER2 and MCF10A-HER2-sFRP cells were treated with SB203580 (5uM) for 24hr. *Axin2* mRNA levels were measured with samples run in triplicate using GAPDH as control. Fold change over control is shown with error bars representing SEM for six biological replicates. **(D)** MCF10A monolayer cultures transfected with pcDNA3 (empty vector) and CAp38α (D176A/F372S, constitutively active mutant) plasmids were treated with Wnt3a conditioned media. *Axin2* mRNA levels were measured following 24 hr of treatment. Fold change over control is shown; error bars=SEM for three biological replicates. **(E)** HER2 and MCF10A-HER2-sFRP cells were cultured in 3D Matrigel and treated from Day 6-12 with DMSO or the p38α/β inhibitor SB203580 (5 μM). The number of acini with outward invading cells was quantified and shown in the graph (n=20 acini/treatment, 2 biological replicates) **(F)** MCF10A-HER2 and MCF10A-HER2-sFRP cells were cultured in 3D Matrigel and treated from days 6-12 with SB203580 (5uM). First and second rows from top panels show representative images of IF staining for E-cadherin (green) and the third and fourth rows show β-catenin (red). Insets in the □-catenin images below (F1-F4) show boxed regions in

higher detail in the fifth row from top to show disruption of β-catenin junctions. Note the rescue of both E-cadherin and β-catenin^{MEM} in sFRP expressing MCF10A-HER2 acini treated with SB203580. Percent of E-cadherin^{HIGH} and β-catenin^{MEM} acini is shown (mean±SEM; n=20 acini/treatment, 2 biological replicates). scale bars=25μM *=p<0.05

Figure 1

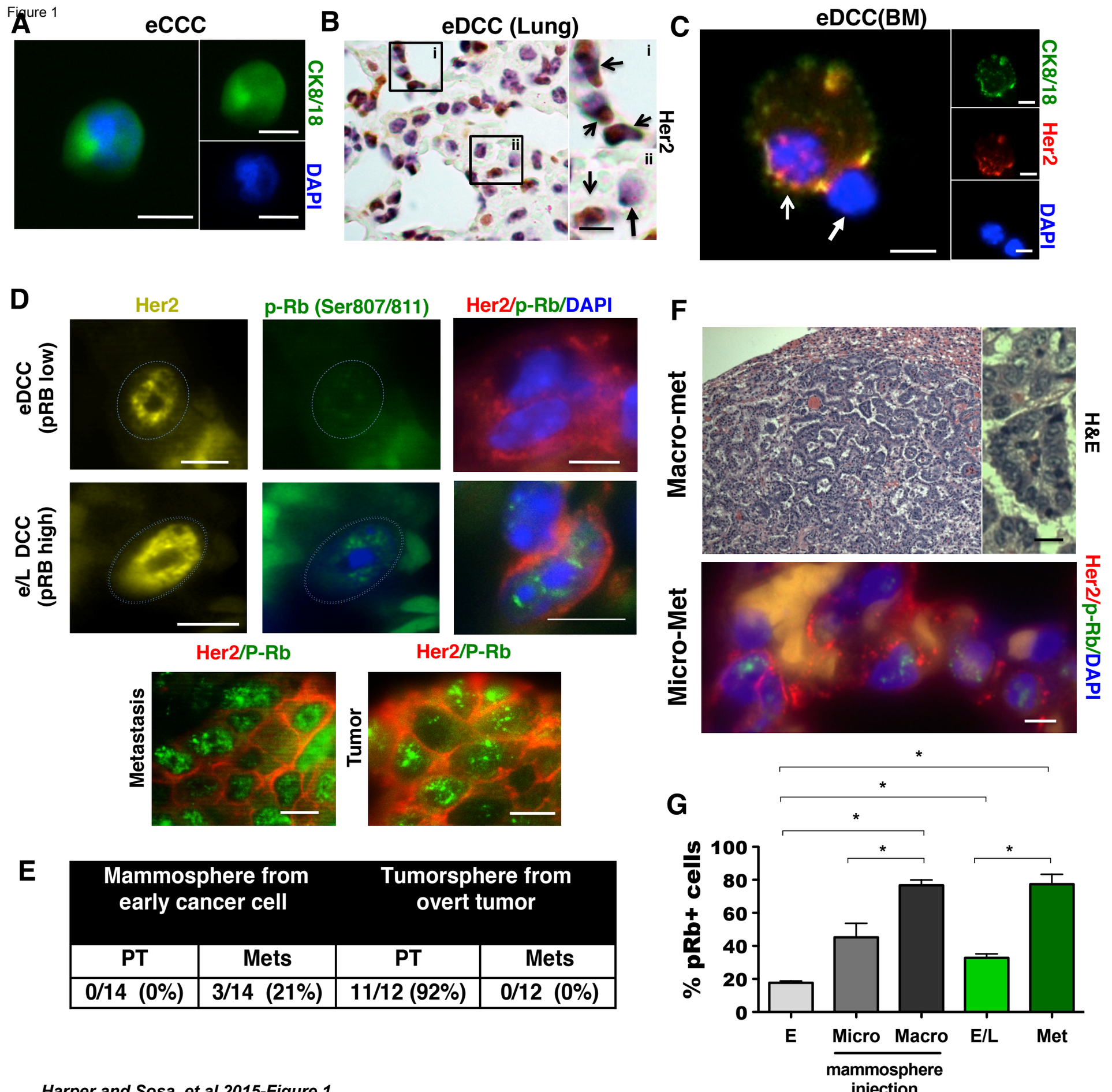

E

Mammosphere from early cancer cell		Tumorsphere from overt tumor	
PT	Mets	PT	Mets
0/14 (0%)	3/14 (21%)	11/12 (92%)	0/12 (0%)

Harper and Sosa et al 2015-Figure 1

Figure 2

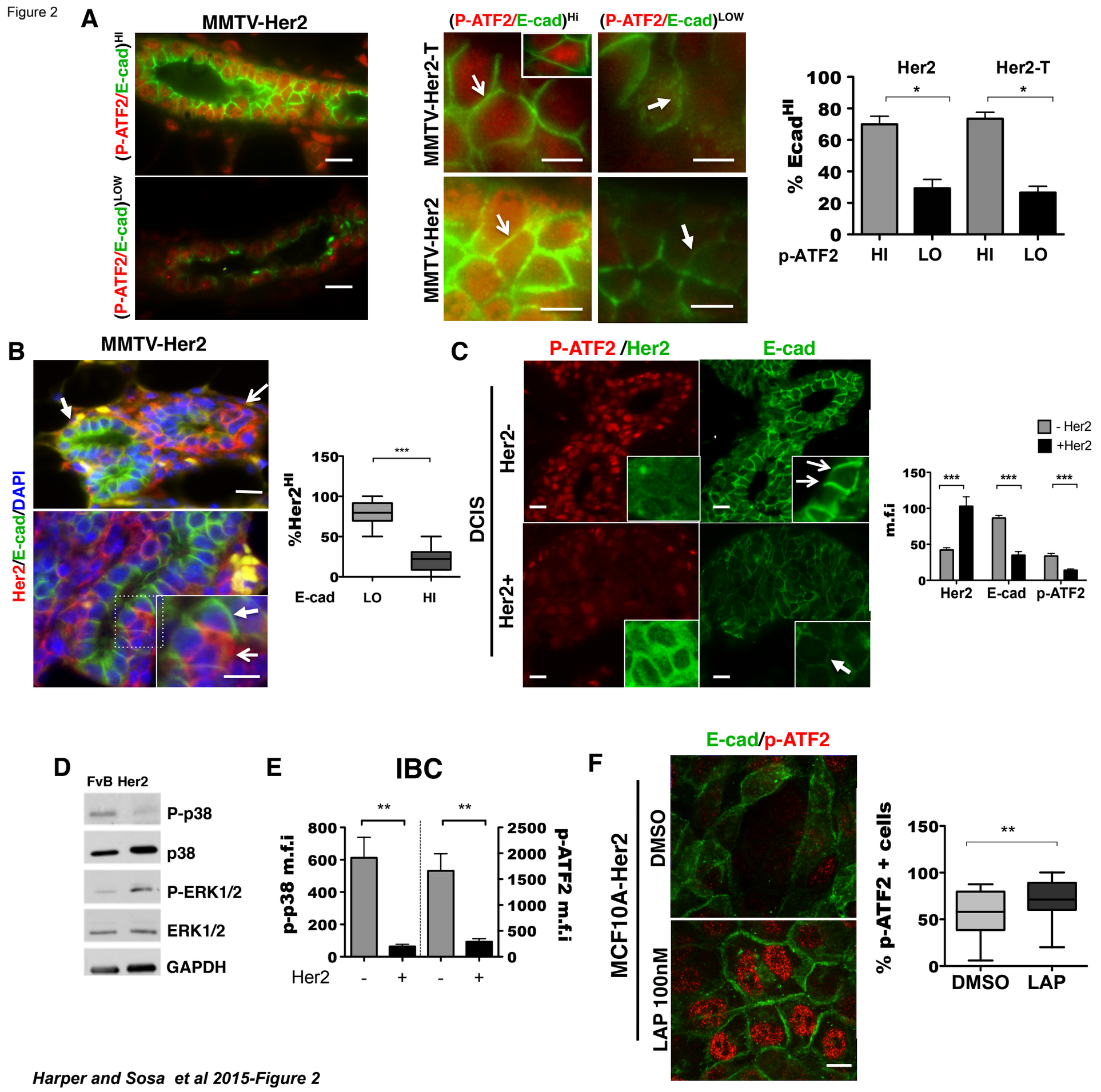

Harper and Sosa et al 2015-Figure 2

Figure 3

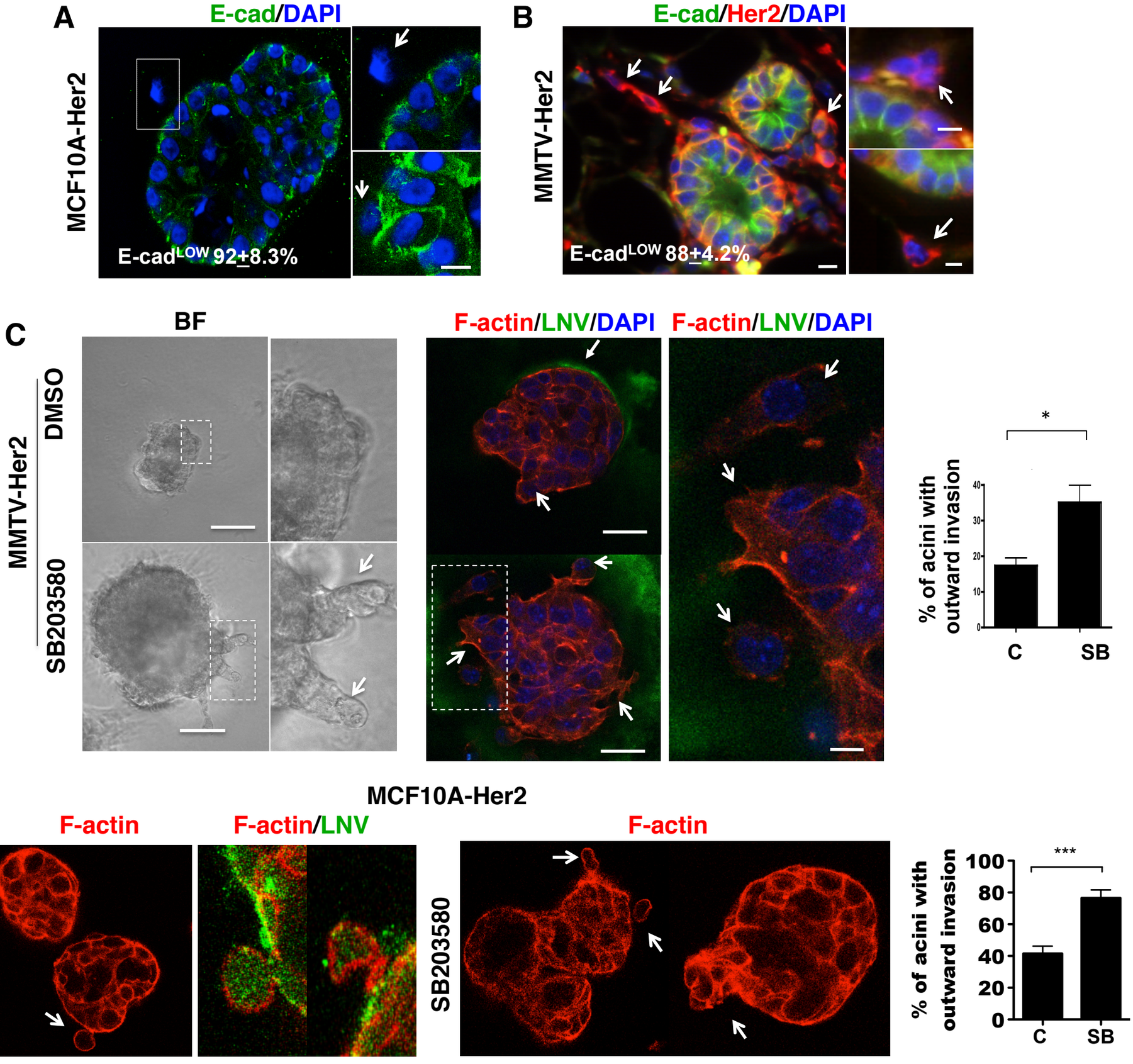

Harper and Sosa et al 2015-Figure 3

Figure 4

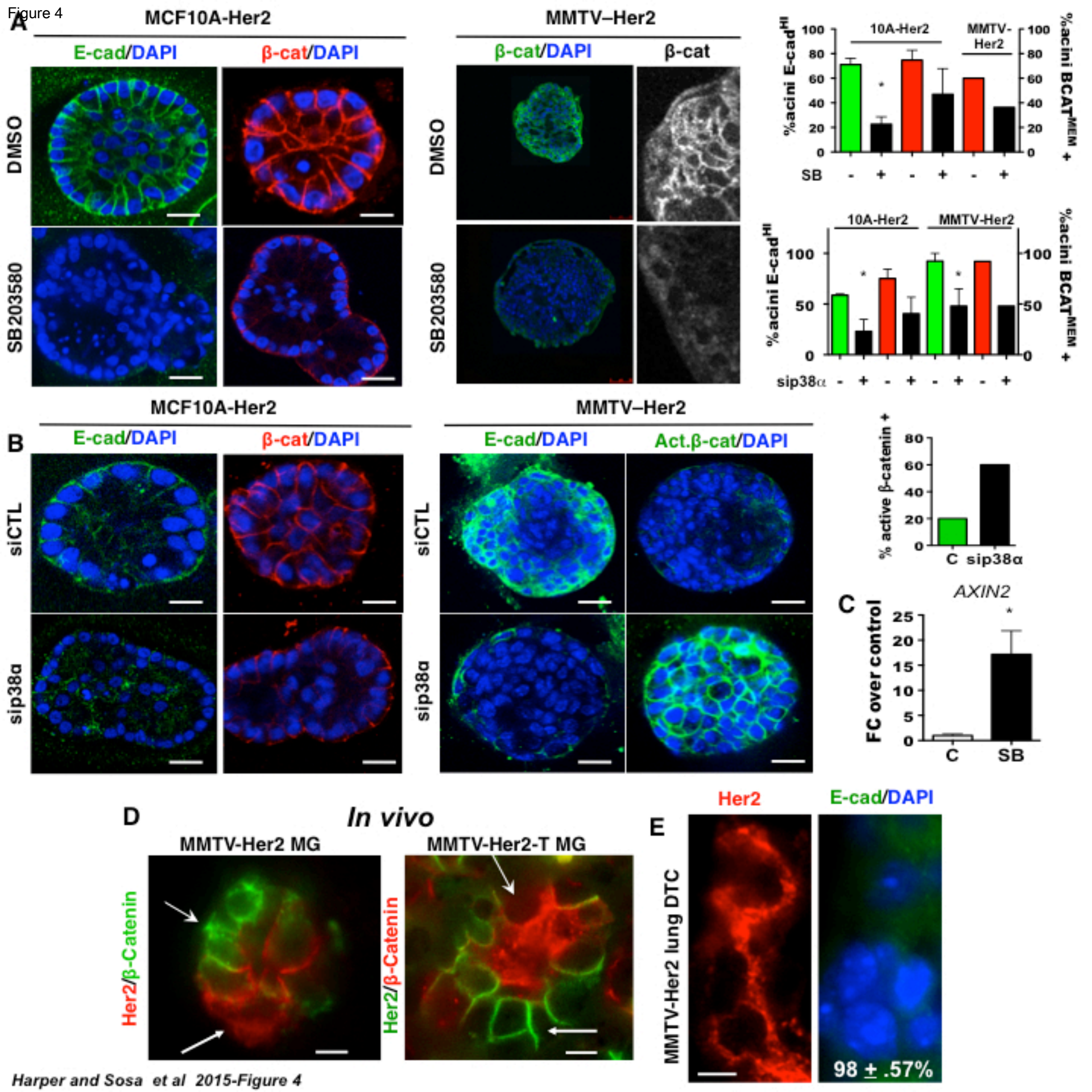

Harper and Sosa et al 2015-Figure 4

Figure 5

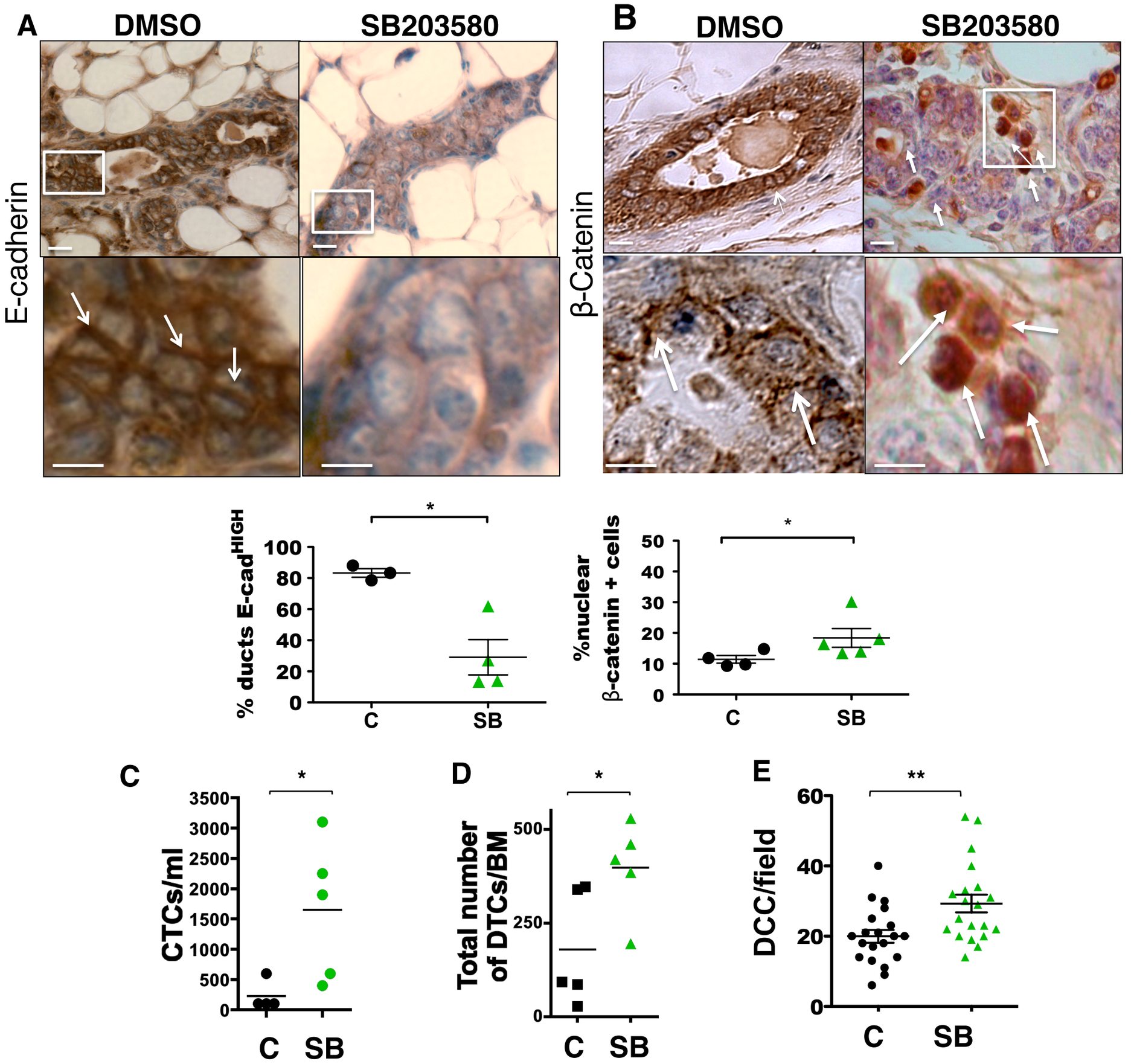

Harper and Sosa et al 2015-Figure 5

Figure 6

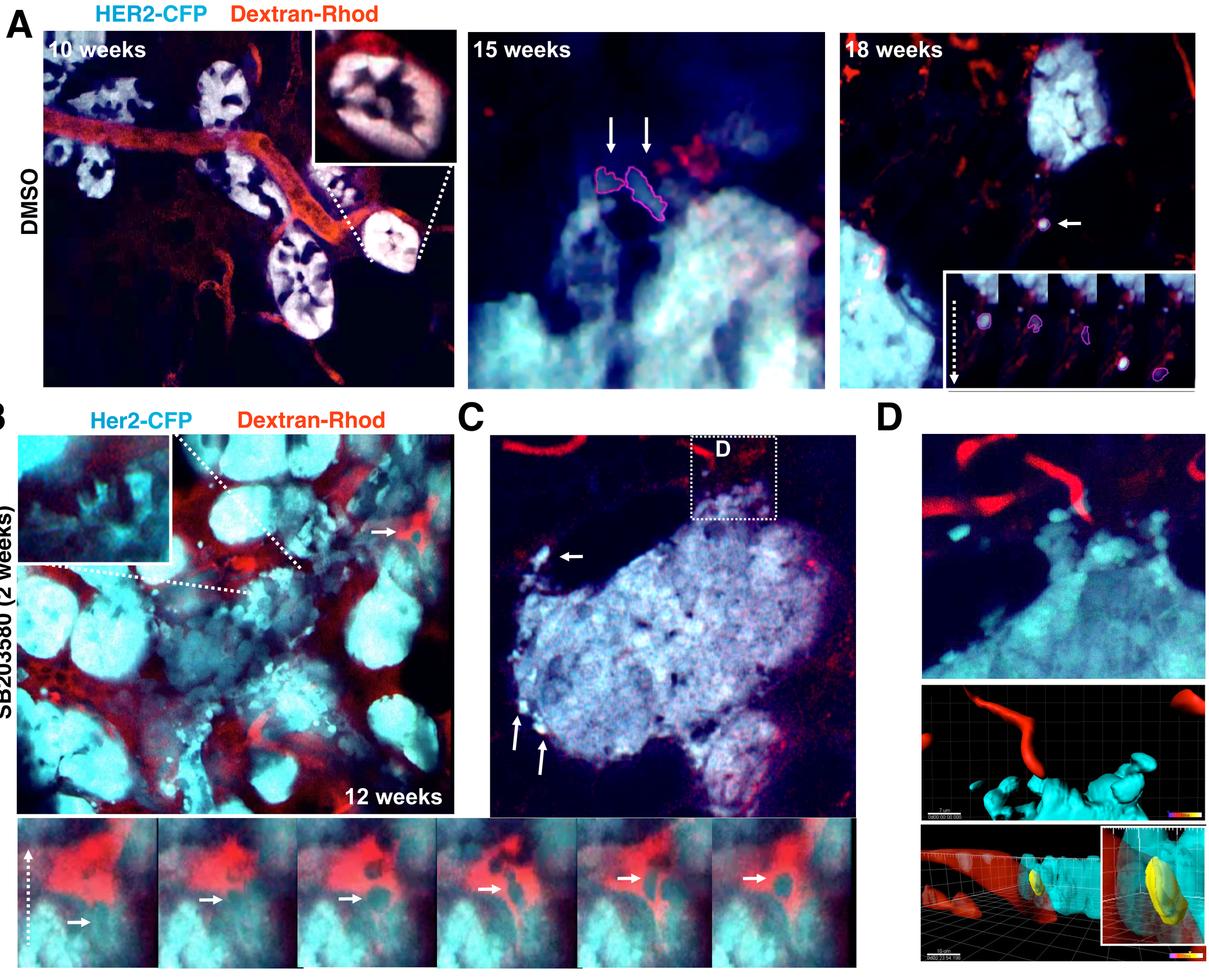

Harper and Sosa et al 2015-Figure 6

Figure 7

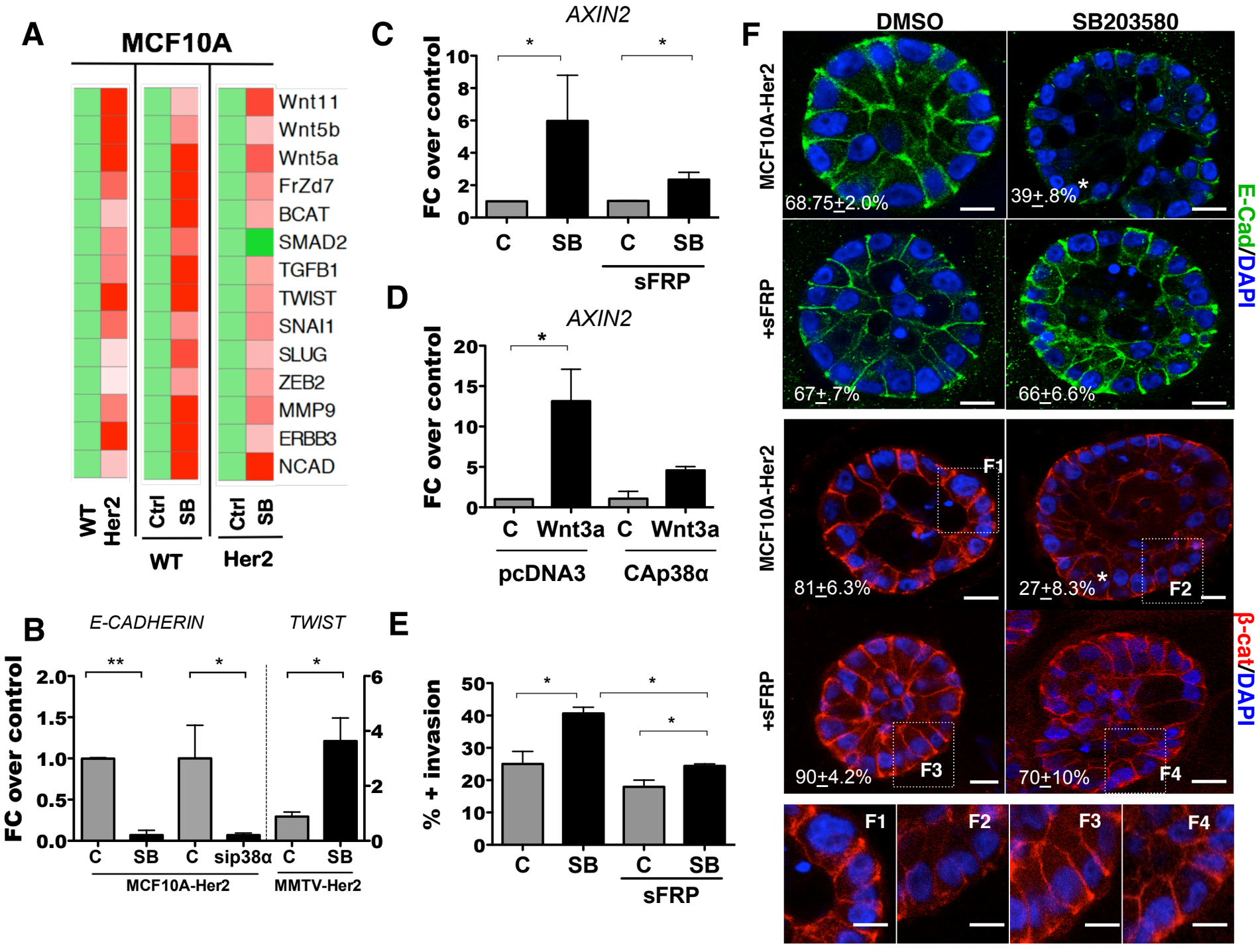

Harper and Sosa et al 2015-Figure 7

Supplemental Figure 1

Click here to download Supplemental Text & Figures: SuppFig1-Harper and Sosa-MS.pdf

A

Disseminating population	Incidence	MMTV-Her2
CCC	100%	225±125 CCCs/ml
DCC BM	100%	180 (Min 28-350 Max) / BM (4 hind limb long bones)
DCC lung	100%	20 (Min 6-40 Max) DTCs/field/section

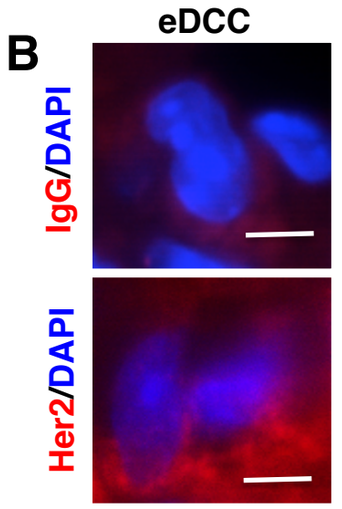

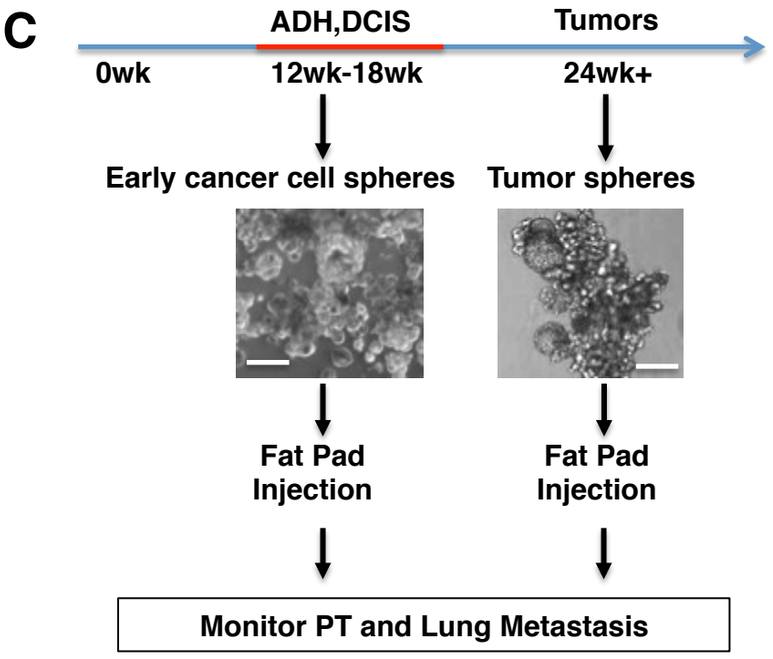

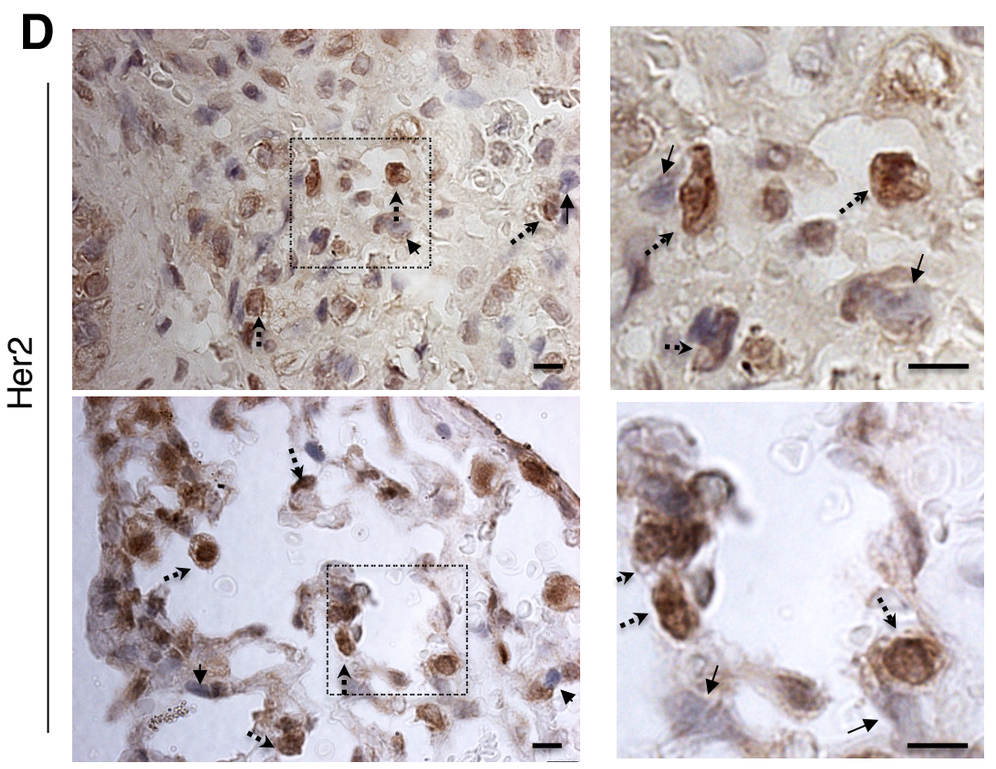

Harper and Sosa et al 2015 - Supplemental Figure 1

Supplemental Figure 2

Click here to download Supplemental Text & Figures: SuppFig2.pdf

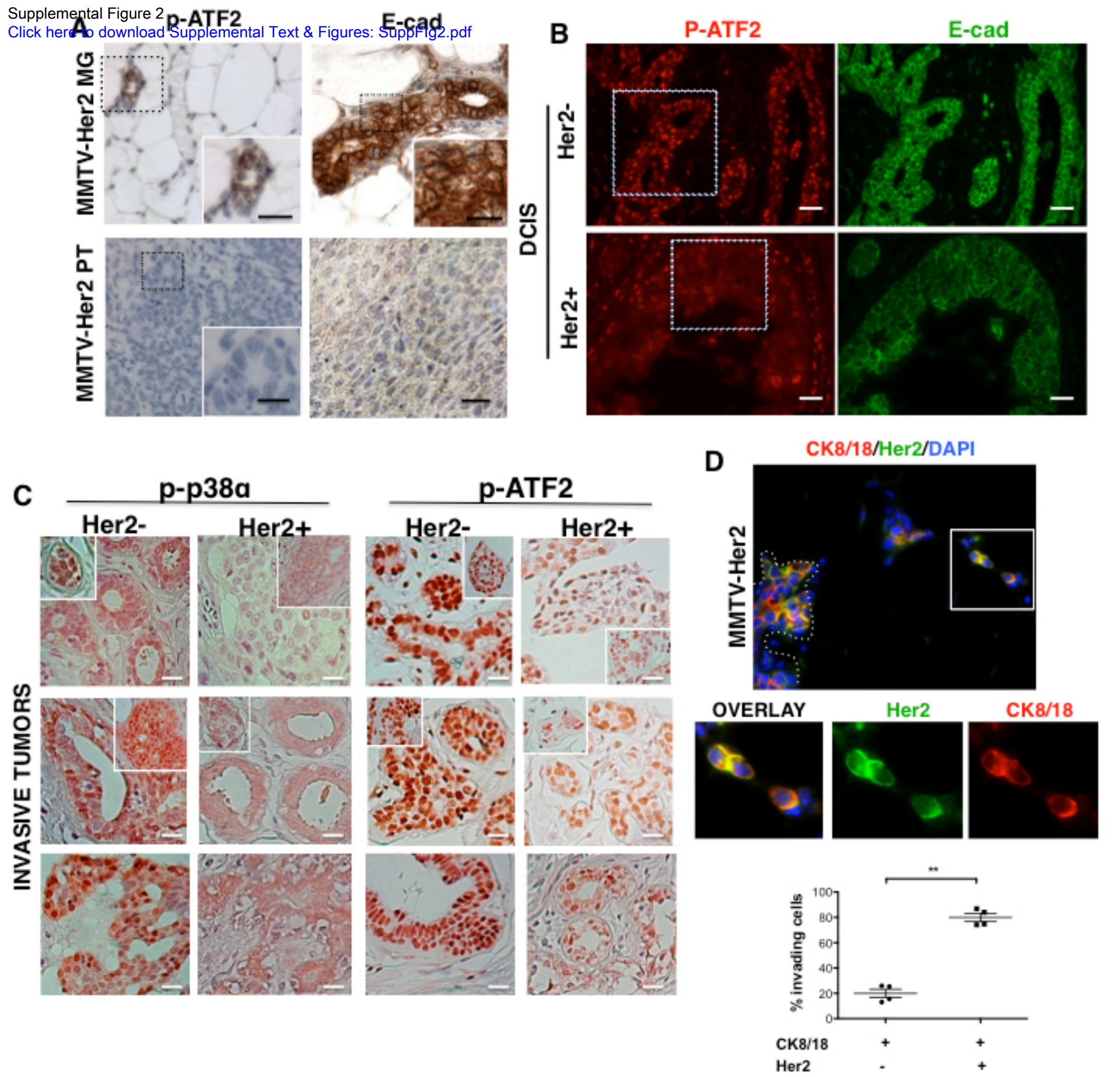

Harper and Sosa et al 2015 - Supplemental Figure 2

Supplemental Figure 3

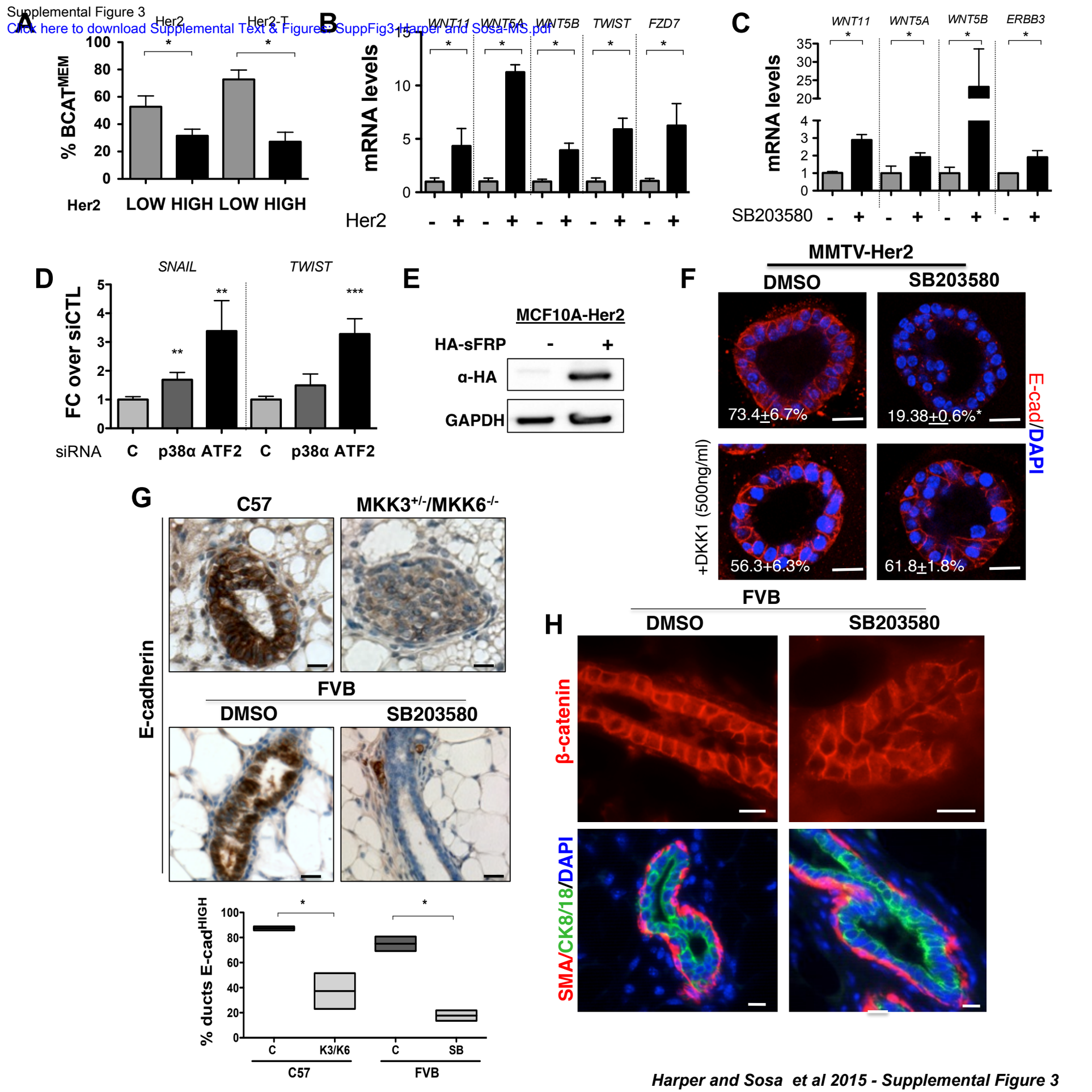

Harper and Sosa et al 2015 - Supplemental Figure 3

SUPPLEMENTAL FIGURE LEGENDS:

Figure S1: DCC with metastatic capacity can be detected in early stage MMTV-HER2 mice and remain pRb negative in target organs

(A) Quantification of the incidence and number of CCCs and DCCs in MMTV-HER2 mice at early stages of cancer progression (age 14-18wk) detected in **Fig 1A-1C** images. CCCs as well as lung and bone marrow DCCs could be detected in 100% of mice as seen in column two of the table (n=4). The mean number of CK8/18+ CCC/mL of blood from cytospin preparations of whole blood samples is shown with SEM (n=4). Bone marrow DTCs were detected as CK8/18+, HER2+ or co-stained for both markers in cytospin preparations from 4 hind long bones (2 tibias, 2 femurs) and the number of DTCs along with minimum and maximum values in the whole bone marrow is shown in the table (n=5). Total counts of BM DTCs are comparable to ~1.3 CK8/18+/HER2+ DTC/million BM cells. The number of lung DTCs per field detected by immunohistochemistry of lungs is shown with minimum and maximum number of DTCs is shown in the table (n=30 fields, 3 mice)

(B) IgG control images for eDCC detection in MMTV-HER2 lung sections. Top panel shows IgG control for HER2 (red). Bottom panel shows example of HER2+ staining. Scale bars=10μM

(C) Experimental set up for mammosphere/tumorsphere injection into fat pad. Briefly, MECs were isolated from the mammary glands of mice at early stages of progression (age 12-18 weeks) as well as from overt tumors and seeded in low adhesion plates in mammosphere media to generate spheres. A representative image of a mammospheres generated from both early and tumor stages is shown. Tumorspheres generated a more golf ball like sphere while early cancer cell structures were more disorganized. ~300 mammospheres were injected into the fat pad of nude mice. Primary tumor formation at the site of injection as well as metastasis was then monitored up to one year. Primary tumor incidence, detection of macro-metastasis and images of resulting metastases are shown in **Fig 1**.

(D) Detection of DTCs in mice that received tumorsphere injections. DTCs were detected using an anti-Her2 antibody. Two representative images of lung sections are shown in left panels with right panels showing zoomed in regions outlined by dashed boxes. Dashed arrows highlight Her2+ DTCs detected in while solid arrows highlight resident Her2- cells within the lung. Scale bar=10μM

(E) Cartoon depicting the three MMTV-HER2 models we have used in this study and the different time scales for early (when ADH and DCIS lesions are present) and over tumor development phases.

Figure S2: HER2 overexpression inhibits p38 signaling and promotes a loss of epithelial identity.

(A) Representative immunohistochemistry images for the downstream p38 kinase target P-ATF2 and E-Cadherin in early MMTV-HER2 (age 14-18wks) mammary glands (MMTV-HER2) and HER2 primary tumor (PT-HER2) sections. Boxed regions are magnified in lower right panel. Note the loss of both P-ATF2 and E-cadherin in primary tumor samples. Scale bar=25μM inset. Insets show details for P-ATF2 and E-cadherin signals.

(B) Lower magnification images of DCIS patient samples stained for p-ATF2 (red) and E-cadherin (green). Boxed area highlights regions shown in **Fig 2.** Scale bar=50μM

(C) Immunohistochemistry using antibodies for P-p38α and P-ATF2 performed on invasive breast cancer tumors from patients. Samples were classified and HER2+ or HER2- by a pathologist after routine IHC performed by the pathology service. Representative images of markers in HER2+/- patients are shown. Note the significant reduction of both p-p38α and p-ATF2 in HER2+ tumors. Insets show additional patient samples for each classification. Quantification of P-p38α and P-ATF2 intensity in samples is shown in **Fig 2** and images in columns represent 5 different patients used in quantifications.

(D) Early MMTV-HER2 mammary gland (age 14-18wk) sections were stained for CK8/18 (red) and HER2 (green), nuclei was counterstained with DAPI (blue). Top image shows a duct outlined with a white dotted line. The boxed region is then shown below with showing CK8/18+ and HER2+ single or

double cells found in within the stroma near ducts. The graph on the bottom shows the average % of these invading cells that were either double positive for both CK8/18 and HER2 or single CK8/18+ with error bars representing SEM. (**=$p<0.01$, n=4mice, 60-80 cells/mouse)

Figure S3: Inhibition of p38 signaling promotes and EMT

(A) Quantification of the percentage of cells with membrane-associated β-catenin ($BCAT^{MEM}$) which were $HER2^-$ or $HER2^+$ as shown in images in **Fig 4D** for FvB MMTV-HER2 and Balb MMTV-HER2-T sections (Her2 and Her2-T). Mean± SEM is shown; MMTV-HER2 30 ducts, 3 mice; MMTV-HER2-T 10 ducts 1 mouse; *=p<0.05

(B) Q-PCR confirmation of selected EMT genes identified in 14-gene EMT signature in **Fig 7A** comparing MCF10A vs. MCF10A-HER2 pre-malignant cells in 3D cultures. Mean ± SEM shown as fold change over control. Values were normalized to GAPDH and samples were run in triplicate.

(C) Q-PCR confirmation of selected genes identified in 14-gene EMT signature in MCF10A-HER2 MECs treated as in **Fig. 7A** with DMSO or SB203580 in 3D matrigel cultures. Mean ± SEM shown as fold change over control. Values were normalized to GAPDH and samples run in triplicate.

(D) mRNA levels were measured for *Snail* and *Twist* in MCF10A-HER2 3D cultures treated with siRNA targeting p38α isoform or ATF2 from Day 6-12. Values represent fold change over control in three biological replicates (2 replicates for siATF2 *SNAIL*). GAPDH was used as housekeeping control.

(E) Western blot analysis confirming expression of HA-tagged sFRP constructs in 10A-HER2-sFRP cell lines. Cell lysates were prepared from 10A-HER2 and 10A-HER2-sFRP expressing cell lines and α-HA was used to detect HA tagged sFRP constructs. GAPDH was used as a loading control.

(F) Early MMTV-HER2 cells (age 14-18wk) were cultured in 3D Matrigel and treated for 2 days with SB203580 (5uM) as well as 500ng/ml DKK1 conditioned media following acini formation. Representative images of immunofluorescence staining for E-cadherin (red) are shown. Numbers in the lower left corners = percent (%) of $E\text{-cadherin}^{HIGH}$ acini (mean± SEM; n=10 acini/treatment, 2 biological replicates *p<0.05). scale bars=25μM

(G) Representative images of immunohistochemistry for E-cadherin in C57 (wt) and $MKK3^{+/-}$ /$MKK6^{-/-}$ mice (Wen et al., 2011) as well as FvB mice treated 2 weeks SB203580 (10mg/kg, i.p every

48hr). Note: even in the absence of the HER2 oncogene both genetic and pharmacological inhibition of p38 signaling results in a loss of E-cadherin. The bottom graph shows the quantification of E-cadherin^{HIGH} ducts in C57-wt, C57-MKK3$^{+/-}$/MKK6$^{-/-}$, and FVB +/- SB203580. Error bars represent SEM, n=2-3 mice. *=p<0.05

(H) *Top row,* immunofluorescence for β-catenin (Red) performed on mammary gland sections of DMSO or SB203580 (10mg/kg, i.p every 48hr) treated FVB mice. Note: β-catenin in FVB mice treated with SB203580 remains localized to the membrane. Scale bar=25μM. *Bottom row*, immunofluorescence for α-smooth muscle actin (SMA, red) and CK8/18 (Green) and nuclei (Blue) on mammary gland sections of DMSO or SB203580 (10mg/kg, i.p every 48hr) treated FVB mice. Note the intact luminal and myoepithelial cell compartments in these ducts following p38α/β inhibition. Scale bar=25μM.

LEGENDS FOR MOVIES

Movie S1: Two-photon imaging of MMTV-HER2-CFP mice at 10 weeks of age. Intra-vital imaging of mammary glands in MMTV-Her2-CFP mice was performed using a specially designed mammary gland imaging window (see Experimental Procedures for details). CFP+ /HER2+ cells can be seen in the cyan/light cyan signal and vasculature was delimited using i.v. delivered dextran-rhodamine (red). Note the apparent normal duct architecture at this time which remained organized with some intra-ductal movement observed mainly in luminal spaces. Still images of movie are shown in **Figure 6A**.

Movie S2: Two-photon imaging of MMTV-HER2-CFP mice at age 15 weeks. Mammary gland imaging windows were used to image ducts of MMTV-Her2-CFP mice at age 15 weeks when early stage lesions (ADH,DCIS) are present. Motile single CFP+ cells were found micro-invading from lesions and are outlined in purple and green in the movie. CFP+/HER2+ cells can be seen in cyan and vasculature was stained with dextran-rhodamine (Red). Note that here a greater digital zoom was used to show in detail the motile cells micro-invading from the ductal structure that occupies the lower right quadrant of the video. Still images of movie are shown in **Figure 6A**.

Movie S3: Two-photon imaging of MMTV-HER2-CFP mice at age 18 weeks. Mammary gland imaging windows were used to image ducts of MMTV-HER2-CFP mice at age 18 weeks when early stage lesions are present. Single cells can were found disseminating from the early stage ducts (upper right) as outlined in in purple in the movie. One single cell can be traced through the stroma between ducts. CFP+/HER2+ cells can be seen in cyan and vasculature was stained with dextran-rhodamine (red) which also revealed macrophages that capture the labeled dextran. Still images of movie are shown in **Figure 6A**.

Movie S4: Systemic p38α/β inhibition in MMTV-HER2-CFP mice stimulates invasion in early cancer cells. MMTV- HER2-CFP mice (10 weeks old) were treated for two weeks with SB203580 (10mg/kg, i.p every 48hr) (12 weeks old at imaging). Compared to control ducts (**Movie S1-3**)

SB203580 treated animals showed ducts with a dramatic increase in luminal filling, and loss of ductal structure. We also detected obvious intra-ductal cell motility and movement along ductal walls (large diagonal duct from center to upper right quadrants). Cells with protrusions are also observed along the top region of the large diagonal duct and in the very top region of this same duct. More detailed movies of invasive events are shown in **Movie S5.** Still images of movie are shown in **Figure 6B** where the descriptions above are indicated.

Movie S5: Intravasation can be detected in MMTV-HER2-CFP mice treated with the p38α/β inhibitor SB203580. Digital Magnification of the Movie S4 and region r indicated in Figure 6B with an arrow. This movie reveals 2-3 CFP+ cells entering the vasculature from the stroma in SB203580 treated mice. *Left panel* shows original imaging. *Right panel* shows vasculature outlined in yellow and intravasating cell outlined in purple for easier visualization. Still images of this sequence are shown in **Figure 6B**, lower series.

Movie S6: Intra-vital imaging of multiple micro-invasion events in MMTV-HER2-CFP mice treated for two weeks with SB203580. Imaging of MMTV-Her2-CFP mammary glands following treatment for two weeks with SB203580 (10mg/kg, i.p every 48hr). This movie shows an ADH/DCIS-like lesion and CFP+/HER2+ cells in cyan and vasculature stained with dextran-rhodamine (red). Note the increased luminal filling of ducts and increased movement of cells along the ductal walls into the stroma and into a low contrast vessel between the two lobules of the ductal structure. See the still images of movie in **Figure 6C** for orientation.

Movie S7: A magnified region from Movie S6 that immobilizes the blood flow by digital averaging of the rhodamine signal highlights the dramatic increase in movement of early cancer cells after p38α/β inhibition systemically cells towards the stroma.

Movie S8: Digital magnification of the region of Movie S7 highlighted in a dotted line square in Figure 6C (inset D). Note the amoeboid like movement of these micro-invading cells breaking the lesion boundaries into the stroma. Note also that the motility seem to occur at the single cell level and not collectively. Single disseminating cells were now found to stream toward the vasculature. Still images of movie are shown in **Figure 6D**.

Movie S9: 3D rendering of the micro-invasion events in MMTV-HER2-CFP mice treated with the p38α/β inhibitor SB203580. 3D reconstruction of **Movie S8** revealed that CFP+/HER2+ cells were potentially accessing the lumen of the blood vessel (RED) as revealed by the yellow overlap signal and suggesting active intravasating capacity as supported by the movies S5 and the detection of CTCs and DTCs in Figure 5. Potential access to the vessel lumen is marked when CFP+ and Dextran-Rhodamine (Red) signals overlap shown in yellow. Still images of movie are shown in **Figure 6D**.

SUPPLEMENTAL EXPERIMENTAL PROCEDURES

Cell culture and cell lines. MCF10A-HER2 cell lines(Sequeira et al., 2009) were cultured using a protocol previously described for MCF10A cell lines (Debnath et al., 2003). HER2 expressing cells were selected for by the addition of G418.

Three-Dimensional Cultures. MCF10A-HER2 cells were cultured in three-dimensional cultures as previously described (Debnath et al., 2003, Debnath et al., 2005). Briefly, cells were seeded in 400ul Assay Media consisting of DMEM/F12, 5% HS, 1% P/S and EGF on 40ul Matrigel (Corning) in 8 well chamber slides (Falcon 354108). Cultures were treated every 24 hours starting at day 6 with 5μM SB203580 (Calbiochem, 559395). $6x10^3$ cells were seeded for immunofluorescence studies and were fixed at day 12 with 4%PFA or 10% Formalin with phosphatase and protease inhibitors ($NaVO_3$, NaF, Pepstatin A, Leupeptin, Aproptinin). To measure mRNA changes in 3D cultures $5.0x10^4$ cells were seeded in 1mL Matrigel in a 24-well plate and RNA was extracted from cultures at day 12 using 1mL Trizol (Ambion 15596018) followed by RNA extraction.

Immunofluorescence. Three-Dimensional cultures were fixed with 4% PFA for 20min at room temperature in the presence of phosphatase and protease inhibitors. Staining was performed as previously described for MCF10A 3D cultures (Debnath et al, 2003). Briefly, cells were permeabilized using .1% Triton X-100 for 20min. Blocking was done using 1x IF wash buffer + 10% Normal Goat Serum (Gibco, PCN5000) for one hour. Primary antibodies used were; for E-cadherin, BD Biosciences #610181; for beta-catenin, BD biosciences #610153; for Laminin V, Progen #10765; for F-Actin, Life Technologies #A12380; for SMA, Sigma #C6198. The following secondary antibodies were used; Alexaflour goat anti mouse 488, Alexaflour goat anti rabbit 568. Chambers were removed from slides and wells were fixed and mounted with ProLong® Gold Antifade reagent with DAPI (Invitrogen P36931). Two-dimensional cultures were fixed with 4% PFA for 20min at 4°C. Cells were permeabilized in .1% Triton-X 100 and then blocked in 3% Normal Goat Serum for 30 min at RT. Primary antibodies were left 1hour at RT in .1% BSA in PBS followed by an additional blocking step. Secondary antibodies were left 1hour at RT in .1% BSA in PBS. Cover slips were fixed using ProLong Antifade mounting media with DAPI (Molecular Probes P36930). Primary antibodies used were; for E-cadherin, BD Biosciences, 610181, and p-ATF2, Cell signaling, 9226.

Immunohistochemistry and Immunocytochemistry. Tissues were fixed in 10% formalin, paraffin-embedded and cut into 4-6μm sections. Following dehydration of the slides antigen retrieval was done in 10mM Citrate Buffer pH 6.0 ($Na_3H_6H_5O_7$). Blocking was done using .1% BSA in PBS with 10% Normal Goat Serum for 30 minutes. Primary antibodies were left overnight at 4°C. The following primary antibodies were used to perform staining; for E-cadherin, BD Biosciences, 610181; for beta-catenin, BD biosciences, 610153; for HER2/HER2, Abcam, ab2428. VectaStain Elite ABC Rabbit IgG (PK-6101) and Mouse IgG (PK-6102) kits from Vector Laboratories were used for secondary antibodies. Secondary antibodies were left for one hour at room temperature. DAB substrate kit (Vector Laboratories, SK-4100) was used for enzymatic substrate. Mounting was done using VECTASHIELD mounting media (Vector Laboratories, H-1400). Tissues were fixed in 10% formalin, paraffin-embedded and cut in 4-6um sections. For Balb-HER2-T staining, paraffin embedded Balb-c and Balb-HER2-T mammary gland and tumors sections were gifted from Dr. Christoph Klein, University of Regensburg, Regensburg Germany. Following dehydration of the slides antigen retrieval was done in 10mM Citrate Buffer ($Na_3H_6H_5O_7$). Triton x-100 was used to permeabilize cells and blocking was done using .1% BSA in PBS with 10% Normal Goat Serum or Normal Donkey Serum (Sigma D9663). Primary antibodies were left overnight at 4°C and secondary antibodies were left for one hour at room temperature. The following primary antibodies were used; for E-cadherin, BD Biosciences, 610182; for beta-catenin, BD biosciences, 610153; for HER2, Abcam, ab2428; for p-ATF2, Cell Signaling, 9226; for pRB (Ser249/Thr252), Santa Cruz, sc-16671 and for CK8/18, Progen 412121. The following secondary antibodies were used Alexaflour 488 goat-anti mouse, Alexaflour 568 goat-anti rabbit, Alexaflour 488 donkey-anti goat, Alexaflour 547 donkey anti rabbit. Slides were mounted using Prolong Antifade mounting media with DAPI (Molecular Probes P36930).

Western Blot. Samples were collected in 1xRIPA buffer and centrifuged at 4°C, 12000rpm to clarify lysate. Protein concentration was used using BioRad Protein Assay Dye Reagent (BioRad 500-0006) and a standard BSA curve. Samples were then boiled for 5 min at 95°C in sample buffer (.04M Tris-HCL pH 6.8, 1%SDS, 1% β-mercaptoethanol and 10% glycerol). 6-10% SDS-PAGE gradient gels were run in Running Buffer (25mM Tris, 190mM glycine, .1% SDS) and transferred to PVDF membranes in Transfer Buffer (25mM Tris base, 190mM glycine, 20% methanol). Membranes were then blocked in 5% milk+ TBST buffer. Primary antibodies

were left overnight at 4°C. Following washing with TBST buffer HRP conjugated secondary antibodies were left at room temperature for one hour. Western blot development was done using Amersham ECL Western Blot Detection (GE, RPN 2106) and GE ImageQuant LAS 4010. Primary antibodies used were; p-p38, BD Biosciences, 612281; p38, BD Biosciences, 612169; p-ERK1/2, Cell Signaling, 9101; ERK, BD Biosciences,610031, GAPDH (Calbiochem, CB1001).. Secondary antibodies used were Peroxidase Horse Anti-Mouse IgG (Vector Laboratories, PI2000; Biotinylated Goat Anti-Rabbit IgG (Vector Laboratories, BA-1000).

EMT qPCR array. RNA was extracted from three-dimensional cultures using Trizol extraction as per manufactures recommendations. cDNA was synthesized using Qiagen RT^2 First Strand Kit (Qiagen 330401). Expression of EMT genes was measured using Qiagen human Epithelial to Mesenchymal Transition PCR array(Qiagen PAHS-090Z)and RT^2 qPCR Master Mixes (Qiagen 330521). Plates were run in an ABI PRISM 7900HT sequence detection system. Results were analyzed using web based PCR array data analysis software provided through Qiagen. Heat maps were generated based on triplicate runs of the array using GENE-E software (Brode Institute).

Q-PCR. RNA was extracted from 2D and 3D cell cultures using Trizol following provider's recommendation. For pre-malignant mammary gland tissue RNA was extracted using Qiagen's RNeasy Lipid Tissue Midi Kit (Qiagen 74804). 2μg RNA was retrotranscribed into cDNA using MMuLV Reverse Transcriptase (New England Biolabs, M0253L), MMuLV buffer (NEB, B0253S) and RNase inhibitor (Ambion, AM2682). Quantitative real time-PCR was performed using Sybr Green Powder PCR Master Mix (Bio-Rad, 170-8882) or preparing master mix using Sybr green (Sigma-Aldrich, S9430), MgCl2(NEB, B9021S), dNTP(NEB N0447L) and taq DNA polymerase(Sigma D6558) in Biorad thermocycler. *Gapdh* was used as housekeeping control for all plates.

Q-PCR Primers

Human- GAPDH forward primer 5'-GGTGAAGGTCGGAGTCAACGG-3',*GAPDH* reverse primer 5'-ATGAAGGGGTCATTGATGGCAACAA-3'; *E-cadherin* forward primer 5'- ATGGGGTCTTGCTATGTTGC -3', *E-cadherin* reverse primer 5'- AAGGCAGAAGGATTGCTTGA -3'; *Twist* forward primer 5'-

GTCCGCAGTCTTACGAGGAG-3',*Twist* reverse primer 5'-CCAGCTTGAGGGTCTGAATC-3'; *SNAI1* forward primer 5'-AGAGCTGACCTCCCTGTCA-3';*SNAI1* reverse primer 5'-TGAAGTAGAGGAGAAGGACGAA-3'; *Wnt11* forward primer 5'- CATGGAGCTCTGCTTGTGAA-3'; *Wnt11* reverse primer 5'-GCTTCCAAGTGAAGGCAAAG -3'; *Wnt5A* forward primer 5'- GAAATGCGTGTTGGGTTGA-3'; *Wnt5A* reverse primer 5'- AGGCATGGGTTTCCATTCT -3'; *Wnt5B* forward primer 5'- CCAAAGGATCAGAGGAGCAG-3'; *Wnt5B* reverse primer 5'- CTCGTTGTTTTGCAGGTTCA-3'; *Erbb3* forward primer 5'-GGCGGCACTTTTCTCTACTG-3'; *Erbb3* reverse primer 5'- CGTTCCAAGTATCGCCTCAT-3'; *FrD7* forward primer 5'-TGGGTTAATTTCCAFFTCA-3'; *FrD7* reverse primer 5'-GCAGTACGGGAGGAAAAACA-3' *Axin2* forward primer 5'-CTGGTGCAAAGACATAGCCA-3'; *Axin2* reverse primer 5'-GTCCAGCAAAACTCTGAGGG-3'

Mouse- *GAPDH* forward primer 5'-AACTTTGGCATTGTGGAAGGGCTC-3'; *GAPDH* reverse primer 5'-TGGAAGAGTGGGAGTTGCTGTTGA-3';*Twist* forward primer 5'-AACTGGCCTGCAAAATCATA -3';*Twist* reverse primer 5'-ACACCGGATCTATTTGCATT-3'

2-photon intra-vital microscopy of mammary glands.

For this work a single laser source tuned to 880nm provided excitation for both the CFP tumor cells and the 155kD rhodamine-dextran vascular label as well as producing a second harmonic generation signal from collagen fibers. Imaging was done with a 25x 1.05NA (XLPL25XWMP2, Olympus) water immersion objective lens so as to bridge between low-magnification visualization of the ductal tree and high resolution single cell imaging. For each mouse, three separate fields were imaged at a time at 5um z steps to a depth of ~50um, with each stack taken approximately every 2min for 4-6hours. Images were reconstructed and analyzed either in ImageJ (Schneider, C.A., Rasband, W.S., Eliceiri, K.W. "NIH Image to ImageJ: 25 years of image analysis". Nature Methods 9, 671-675, 2012.), utilizing the custom written ImageJ plugin, ROI_Tracker (Entenberg et al., 2011) or with Imaris (Bitplane). Mice were anesthetized using 0.75 – 2.5% isofluorane, depilated, and a skin flap surgery performed exposing the 2nd and 3rd mammary fat pad. The absence of a solid tumor presents necessitated the development of a custom fixturing technique wherein the exposed fat pad was affixed with cyanoacrylate glue to the edge of a 15mm window fitted with a 12mm diameter coverglass. The window was captured on a fixturing plate placed on the microscope xy stage and imaging was performed in the center of

the window away from the glue. Animals were maintained at physiological temperatures throughout imaging with an AirTherm ATX forced air heater (WPI Inc.) and supplemented i.v. with 50-100uL of PBS per hour. Any residual x-y drift not eliminated by the fixturing window was removed with post processing using the StackReg plugin (P. Thévenaz, U.E. Ruttimann, M. Unser IEEE Transactions on Image Processing, vol. 7, no. 1, pp. 27-41, January 1998) for ImageJ.

Supplemental Movie 1

Click here to download Supplemental Movies & Spreadsheets: Movie S1-Ctrl-10wks.mov

Supplemental Movie 2

Click here to download Supplemental Movies & Spreadsheets: Movie S2-Ctrl-15wks.mov

Supplemental Movies 3

Click here to download Supplemental Movies & Spreadsheets: Movie S3-Ctrl-18wks.mov

Supplemental Movie 4

Click here to download Supplemental Movies & Spreadsheets: Movie S4-SB-2wks-field.mov

Supplemental Movie 5

Click here to download Supplemental Movies & Spreadsheets: Movie S5-SB-2wks-intravasation.mov

Supplemental Movie 6

Click here to download Supplemental Movies & Spreadsheets: Movie S6-SB-2wks-invasionfield.mov

Supplemental Movie 7

Click here to download Supplemental Movies & Spreadsheets: Movie S7-SB-2wks-invasion-intravasation.mov

Supplemental Movie 8

Click here to download Supplemental Movies & Spreadsheets: Movie S8-SB-2wks-invasion.mov

Supplemental Movie 9

Click here to download Supplemental Movies & Spreadsheets: Movie S9-SB-3Drec.mpg